Basin Research

IAS EAGE

Basin Research (2011) **23**, 171–190, doi: 10.1111/j.1365-2117.2010.00489.x

Holocene mass-wasting events in Lago Fagnano, Tierra del Fuego (54°S): implications for paleoseismicity of the Magallanes-Fagnano transform fault

Nicolas Waldmann,*† Flavio S. Anselmetti,‡ Daniel Ariztegui*, James A. Austin, Jr,§ Mortaza Pirouz*, Christopher M. Moy¶ and Robert Dunbar||

*Section of Earth and Environmental Sciences, University of Geneva, Geneva, Switzerland

†Department of Earth Science, University of Bergen, Bergen, Norway

‡Eawag, Department of Surface Waters, Swiss Federal Institute of Aquatic Science and Technology, Duebendorf, Switzerland

§Institute for Geophysics, John A. and Katherine G. Jackson School of Geosciences, University of Texas at Austin, TX, USA

¶Geology Department, University of Otago, Dunedin, New Zealand

||Department of Geological and Environmental Sciences, Stanford University, Stanford, CA, USA

ABSTRACT

High-resolution seismic imaging and coring in Lago Fagnano, located along a plate boundary in Tierra del Fuego, have revealed a dated sequence of Holocene mass-wasting events. These structures are interpreted as sediment mobilizations resulting from loading of the slope-adjacent lake floor during mass-flow deposition. More than 19 mass-flow deposits have been identified, combining results from 800 km of gridded seismic profiles used to site sediment cores. Successions of up to 6-m thick mass-flow deposits, pond atop the basin floor and spread eastward and westward following the main axis of the eastern sub-basin of Lago Fagnano. We developed an age model, on the basis of information from previous studies and from new AMS-^{14}C ages on cored sediments, which allows us to establish a well-constrained chronologic mass-wasting event-catalogue covering the last ~12 000 years. Simultaneously triggered, basin-wide lateral slope failure and the formation of multiple debris flow and postulated megaturbidite deposits are interpreted as the fingerprint of paleo-seismic activity along the Magallanes-Fagnano transform fault that runs along the entire lake basin. The slope failures and megaturbidites are interpreted as recording large earthquakes occurring along the transform fault since the early Holocene. The results from this study provide new data about the frequency and possible magnitude of Holocene earthquakes in Tierra del Fuego, which can be applied in the context of seismic hazard assessment in southernmost Patagonia.

INTRODUCTION

Lake sediments have been demonstrated to reliably record both past climatic events (e.g. Prentice *et al.*, 1992) and modern anthropogenic influences (e.g. Bookman *et al.*, 2008). Moreover, during the past few decades, the interest in lacustrine basins as paleoseismic archives has grown, as a result of the potential impact of earthquakes on lake-shore environments and near-shore populations (e.g. Schnellmann *et al.*, 2002; Guyard *et al.*, 2007). Many lakes have evolved in tectonically controlled basins, such as those encountered along plate boundaries. Some of these lakes are typified by sharp breaks between steep lateral slopes and a generally elongated flat basin floor, such as Lake Tanganyika (Scholz & Rosendahl, 1988) and the Dead Sea (Garfunkel, 1981). Because of their proximal locations to ongoing tectonism, the sedimentary record of these plate-boundary lakes is suitable for the analysis of seismically induced structures and thus for paleoseismicity studies (Sims, 1975; Ricci Lucchi, 1995). The geometries of these basins foster the development of depositional environments in which a variety of heterolithic facies develop in response to seismic shaking. The effects of seismic shocks related to fault movements can be imprinted in lacustrine sediments as deformational structures, called seismites, if the seismic events exceed a certain local intensity and/or the lithology and compactional state of the sediments allow liquefaction (Marco & Agnon, 1995; Moretti *et al.*, 1999; Ken-Tor *et al.*, 2001; Monecke *et al.*, 2004, 2006).

Correspondence: Nicolas Waldmann, Department of Earth Science, University of Bergen, Allégaten 41, 5007 Bergen, Norway. E-mail: nicolas.waldmann@geo.uib.no

© 2010 The Authors
Basin Research © 2010 Blackwell Publishing Ltd, European Association of Geoscientists & Engineers and International Association of Sedimentologists

On inclined surfaces, seismic shocks may nucleate slope instabilities, distributing large amounts of slope sediments over wide basinal areas (Masson *et al.*, 2007) and disrupting basinal sediments that are overridden by displaced slope sediments (Schnellmann *et al.*, 2005). Many studies describe subaqueous mass movements induced by historical earthquakes, both in marine (Syvitski & Schafer, 1996; Nakajima & Kanai, 2000; Goldfinger *et al.*, 2003, among others) and lacustrine environments (Siegenthaler *et al.*, 1987; Chapron *et al.*, 1999, among others). Lacustrine basin geometry also plays an important role, by influencing the flow behaviour and depositional characteristics of lateral mass movements (Kelts & Hsu, 1980), and by favouring compression and deformation of flat-lying lake-floor sediments through the impact and load of seismically displaced sediment masses (Schnellmann *et al.*, 2005). Slumps and mass-flows evolve downslope into debris flows and megaturbidites, which together represent significant sediment-accumulation processes in the deeper parts of lakes in tectonically active areas. Applying these concepts, this study attempts to assess the magnitude and recurrence rates of earthquakes in a remote Patagonian region by investigating the Lago Fagnano sedimentary record (Tierra del Fuego, Fig. 1a and b), providing a preliminary step towards gauging the potential seismic hazard to local communities.

STUDY SITE: LAGO FAGNANO

Lago Fagnano is an excellent example of a lake evolving in an interplate basinal system. The origin and evolution of this lake basin represents a combination of glacial and tectonic processes, as this basin developed in a tectonic setting amplified by recurring glacial activity. Lago Fagnano is located at ~54°S in the southern part of Tierra del Fuego Island, southernmost Patagonia (Fig. 1a and b). This lake occupies a deep continental pull-apart basin interpreted to have formed as a result of sinistral movements along the Magallanes-Fagnano transform fault (MFT) since the Miocene (Klepeis, 1994; Lodolo *et al.*, 2003) (Fig. 1a). To date, however, no clear subsurface evidence for a pull-apart origin has been confirmed (Waldmann *et al.*, 2008); yet a deep negative 'flower structure' was proposed as an alternative explanation for the formation of other basins along the MFT (Lodolo *et al.*, 2003). By examining the western part of the MFT transform in the Straits of Magellan, Winslow (1982) proposed that sinistral displacement along the MFT zone amounts to ~80 km. These tectonically induced weakness zones were used preferentially by moving ice during and after the last glacial maximum (LGM) and previous glaciations, when glaciers originating in the Cordillera Darwin to the west (Fig. 1b) advanced along the MFT eastwards (Coronato *et al.*, 2009; Waldmann *et al.*, 2010).

Lago Fagnano consists of two basins separated by a shallow sill: an elongated, ~120-m deep sub-basin in the west and a ~200-m deep sub-basin in the east (Fig. 1c). The greater water depth of the eastern sub-basin suggests either that it has experienced larger amounts of tectonic subsidence (presumably along the MFT) or enhanced glacial erosion. Waldmann *et al.* (2010) have proposed that the elongated western sub-basin was formed as the result of primarily glacial erosion, perhaps intensified by ongoing strike-slip movement along the MFT (Cunningham, 1993). In support of this hypothesis, we have observed recent faulting of the youngest sedimentary infill of the lake (Fig. 2) and we note historic seismicity that could have induced such faulting (Lomnitz, 1970; Costa *et al.*, 2006).

The MFT system crosses Tierra del Fuego in an ~E–W direction, separating the South American and the Scotia plates (Fig. 1a). Seismicity along this transform boundary has been high ($M_w > 7$) and shallow (< 40 km) during the last couple of centuries (Vuan *et al.*, 1999; Febrer *et al.*, 2000). Historically recorded seismic events are limited due to population scarcity in Tierra del Fuego during this period. Only two earthquakes are known: the 2 February, 1879 (M_w = ~7.5) event, with an epicentre in the Straits of Magellan several tens of kilometres west of Lago Fagnano, and the 17 December, 1949 (M_w = 7.8) event, with a similar epicentre location (Lomnitz, 1970). The earthquake that hit Tierra del Fuego in 1949 caused instability and landslides along the banks of Lago Fagnano, triggering the subsidence of large areas along the lake shores that remain visible today (Menichetti *et al.*, 2001; Lodolo *et al.*, 2003). It is further suggested that the 1949 earthquake induced < 1 m of left-lateral fault slip (Costa *et al.*, 2006). This seismic event also influenced areas far from the epicentre, such as the westernmost arm of the Straits of Magellan, where tsunamis were registered (Jaschek *et al.*, 1982). The proximity of the Fagnano basin to these recorded epicentres along the MFT makes the sedimentary infilling of Lago Fagnano a potentially exceptional archive of paleoseismic activity along the transform. With this contribution, we aim to reconstruct the paleo-seismic record on the island of Tierra del Fuego as recorded in the seismic stratigraphy and sedimentary record of the easternmost sub-basin of Lago Fagnano.

METHODS

More than 800 km of geophysical profiles were acquired in 2005 using the *R/V Neecho* within the Argentine portion (~87%) of Lago Fagnano (Fig. 1c). Single-channel, high-resolution 3.5 kHz (pinger) and 1 in^3 airgun, multi-channel seismic data were simultaneously collected. Although the pinger survey, the focus of this study, yields seismic stratigraphic information about shallow subsurface sediments to depths of several tens of meters with theoretical vertical resolution of a few to tens of centimetres, the airgun data image the deeper sedimentary deposits and bedrock morphology of the basin. Results of that survey have been published elsewhere (Waldmann *et al.*, 2008, in press). Seismic profiles were digitally recorded in SEG-Y format, using a non-differential global positioning system (GPS)

© 2010 The Authors

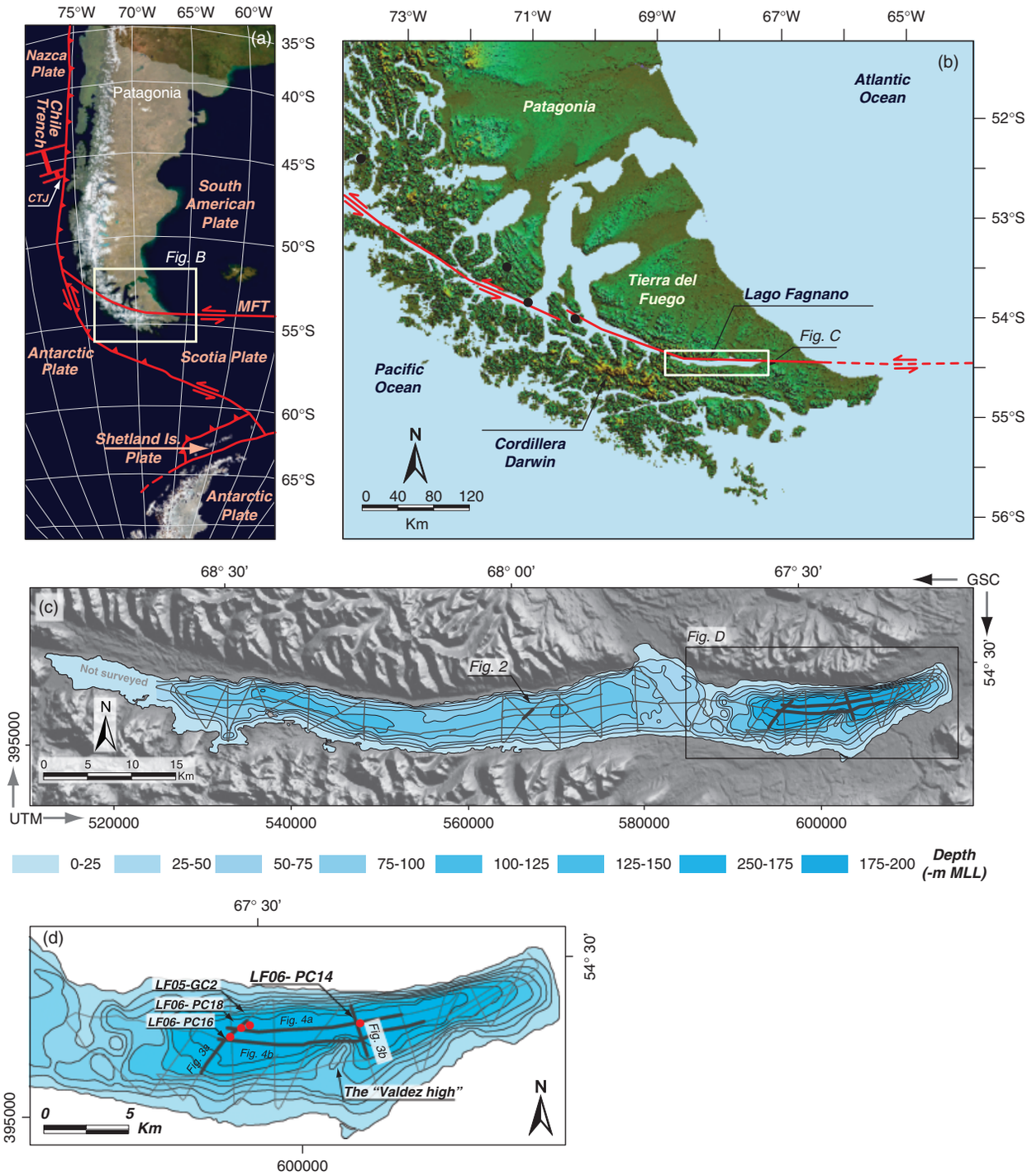

Fig. 1. (a) Satellite map of Patagonia (Hogan, 2009), with the major tectonic provinces and fault boundaries marked in red. CTJ, Chile Triple Junction; MFT, Magallanes-Fagnano Transform system. (b) High-resolution digital elevation model (Mercator projection) from processed National Aeronautics and Space Administration (NASA) Shuttle Radar Topography Mission data (SRTM; Farr *et al.*, 2007) of Tierra del Fuego, with the Lago Fagnano location marked. Continuous and dashed red lines stand for both recognized and suggested delineation of the MFT system (Lodolo *et al.*, 2003). Black dots stand for significant earthquakes ($M_w > 7.5$) since 1800 (http://www.ngdc.noaa.gov/). (c) Bathymetric map of Lago Fagnano developed from seismic data collected during this investigation and preexisting data (Lodolo *et al.*, 2003), showing the seismic profiles plotted over a SRTM map. Contour interval is 25 m. Depth in meters below mean lake level (MLL). (d) Bathymetric map of the eastern sub-basin, showing the seismic profiles and piston and gravity cores described in this paper.

with an average accuracy of ± 5 m. GPS navigation fixes were geo-referenced to previously published maps of Lago Fagnano (Lodolo *et al.*, 2002). Bandpass filtering (2–6 kHz) and automatic gain control (AGC; window length 100 ms) were applied to the pinger data. Diffracted noise attenuation and a water bottom mute were also applied. The mul-

© 2010 The Authors
Basin Research © 2010 Blackwell Publishing Ltd, European Association of Geoscientists & Engineers and International Association of Sedimentologists

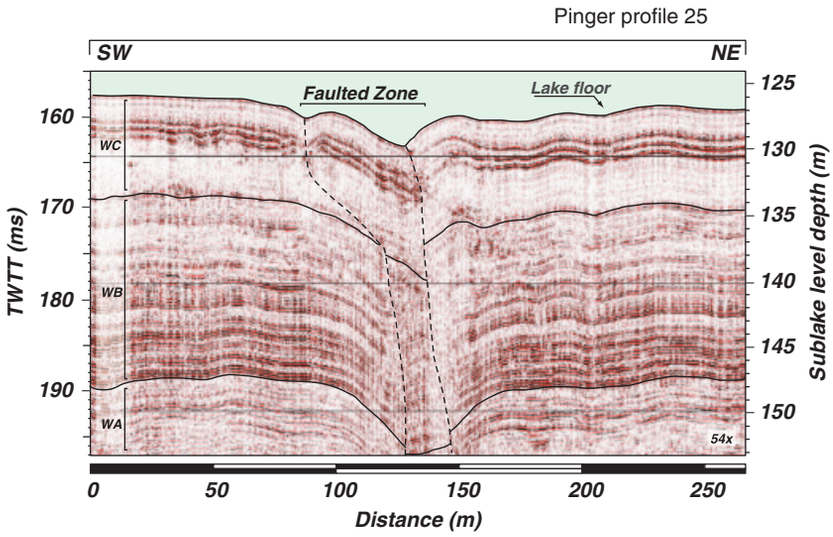

Fig. 2. SW–NE 3.5 kHz seismic profile crossing the western sub-basin (see Fig. 1c for location). Sediment depth is given in milliseconds of two-way traveltime (TWTT) and consequently converted to sub-lake level depth (m) based on a P-wave velocity of 1430 m s^{-1} for water and 1500 m s^{-1} for sediment. We recognize three different seismic units (WA, WB and WC), based on differences in the seismic facies (following Waldmann *et al.*, in press). Notice the interpreted faulted zone fracturing the different seismic units including the lake floor, probably in relation to the MFT zone. Vertical exaggeration is shown in the lower right side of the profile.

tichannel seismic data were interpreted using the Kingdom Suite™ software developed by Seismic Micro-Technology Inc. For time-to-depth conversion, we assumed an average velocity of 1430 m s^{-1} (for the water column) and 1500 m s^{-1} (for the sediments), as calculated in similar sedimentary alpine basins (Finckh *et al.*, 1984).

Gravity and piston-coring sites were targeted at selected locations based on interpretation of the seismic data retrieved during 2005 and 2006 field seasons, again using *R/V Neecho* (Fig. 1d). Gravity cores ~1–2 m in length and Kullenberg-type piston cores up to 8.5 m long were collected. A total of 18 cores were retrieved from the entire lake basin at different depths, but only four with the best sediment recovery from the eastern sub-basin are used in this study. The piston cores were cut into 1.0–1.5 m sections for transport to ETH Zurich and stored in a dark room at 4 °C. They were scanned prior to opening with a GEOTEK™ multi-sensor core logger (MSCL) to obtain the following petrophysical properties: P-wave velocity, γ-ray attenuation bulk density and magnetic susceptibility. Calibration of the MSCL instrument was carried out using an aluminium and water standard. The cores were photographed immediately after splitting and lithologic successions were described visually in detail. Preliminary sampling included smear-slide analysis to characterize sediment types and other major components (e.g. biogenic debris). Elemental determinations in selected samples at ~50 µm resolution (Na to Sr, as limited by the analyzing equipment) were carried out at the University of Geneva, with a non-destructive Röntgenanalytik Eagle II micro X-ray fluorescence system. Acquisition parameters of the Rh tube were set at 40 kV and 800 mA.

A core-to-core correlation has been established using the sequential pattern of interpreted mass-wasting deposits, including their thicknesses, petrophysical properties, laminae counts and lithologic architecture. Laminae correlation from core-to-core has also served to assess the extent of possible erosional surfaces. Isopach maps of the different mass-wasting deposits have also been developed from the interpreted pinger profiles using radial basis interpretation in Arc-Map software (developed by ESRI™). Thicknesses have been confirmed using the core results; the map contours have been extrapolated between profiles using a near-neighbour interpolation included in the software.

SEISMIC STRATIGRAPHY

The grid of high-resolution seismic profiles in the eastern sub-basin of Lago Fagnano has allowed us to visualize the basin infill and to reconstruct the recent seismic stratigraphic architecture of the lake sediments. At a greater scale, the seismic stratigraphic architecture of the Fagnano basin may be comparable to similar marine basins such as fjords (St-Onge *et al.*, 2004; Hjelstuen *et al.*, 2009, among others). Based on different seismic facies, three major seismic stratigraphic units, EA, EB and EC, from bottom to top, respectively, have been distinguished in the eastern sub-basin (Fig. 3). Unit EA is distinguished by a transparent to semi-transparent chaotic seismic facies, with occasional internal medium-energy parallel-continuous reflections. In contrast, overlying unit EB is characterized by discrete bands of equally spaced, continuous, medium-to-high amplitude reflections separating transparent subunits reaching a total thickness of up to 6 m. Topmost unit EC drapes the entire sequence and is typified by intercalations of thinly spaced, high-amplitude internal reflections, with low-amplitude to transparent intervals that get thicker eastwards while becoming more chaotic, reaching thicknesses up to 10 m.

This seismic stratigraphy of the eastern sub-basin differs from the architecture defined for the western sub-basin, which we believe is also primarily glacially derived, but older than the section in the eastern sub-basin (Waldmann *et al.*, 2010). We have interpreted the seismic architecture of the eastern sub-basin to represent glacially derived sediments (EA), overlain by a sequence dominated

© 2010 The Authors

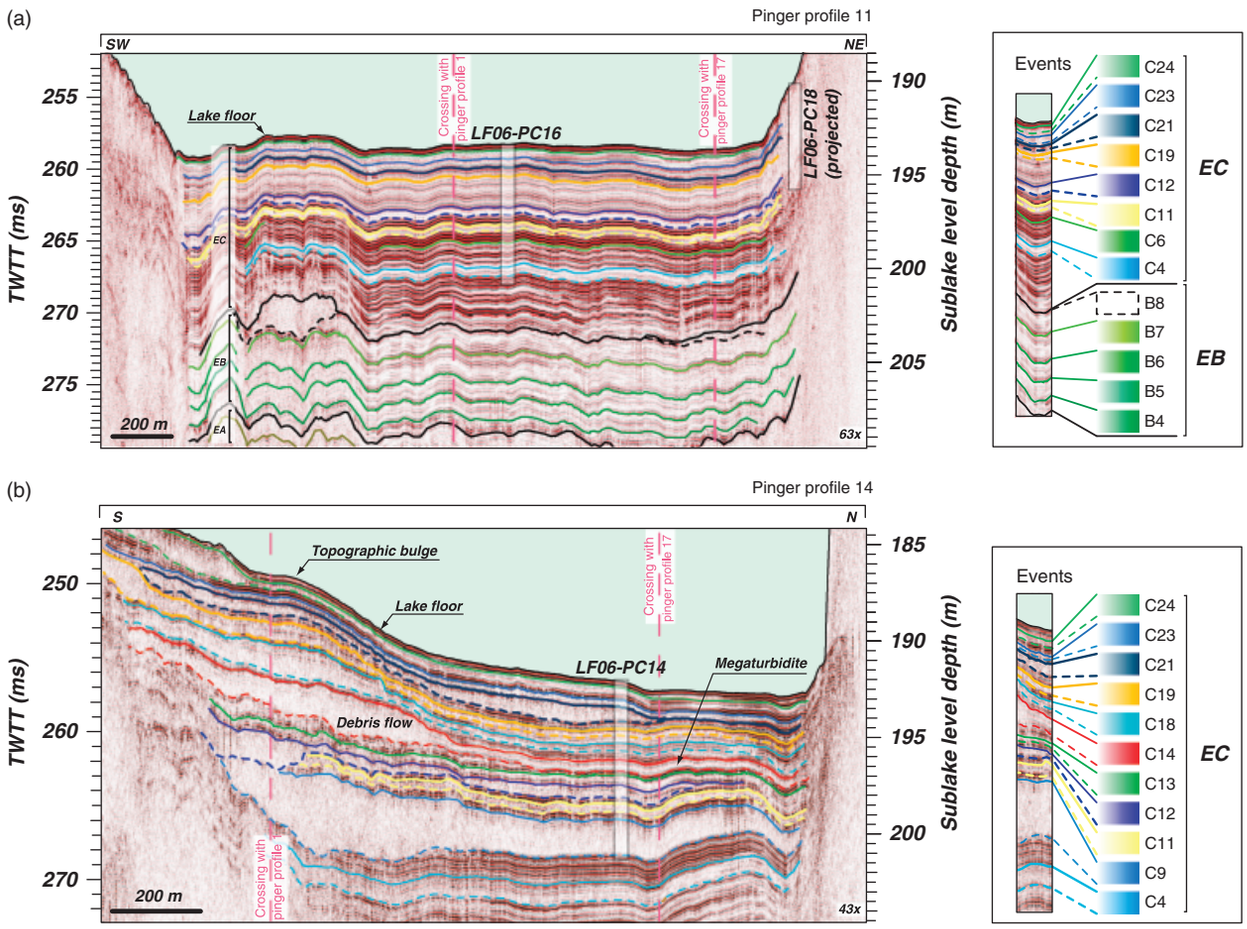

Fig. 3. SW–NE (a) and N–S (b) 3.5 kHz sections crossing the eastern sub-basin (see Fig. 1d for location). Positions of cores are also labelled. EC and EB in the lower figure represent the different seismic units discussed in the text (see also Fig. 2). However, only the uppermost part of seismic unit EA is imaged here. Sediment depth is given in milliseconds of two-way traveltime (TWTT). We convert these travel-times to sub-lake level depth (m) based on a P-wave velocity of 1430 m s^{-1} for water and 1500 m s^{-1} for sediment. The different colour horizons stand for the different mass-flow deposits. Notice the different vertical exaggeration in both profiles. Uninterpreted profiles are published in the supplementary material associated with this article.

by proglacial megaturbidites (EB), which is in turn overlain by a pelagic-style sequence intercalated with downslope mass-flow deposits (EC). The equally spaced semi transparent unit EB was interpreted by Waldmann *et al.* (in press) as sequences of proglacial turbidites or of small slides reflecting sediment pulses released by the retreating Fagnano glacier to the basin during deglaciation. Moreover, they further postulate that the southward thickening of seismic unit EC is mostly caused by lens-shaped, seismically transparent to semi-transparent bodies with concave-up geometries, which represent ponded mass-flow deposits derived from the southern, mountain-facing, flank of Lago Fagnano (Fig. 3). This architecture has been previously recognized in other similar environments such as alpine lake systems in France (Chapron *et al.*, 1996), Switzerland (Schnellmann *et al.*, 2002, 2005; Strasser *et al.*, 2007; Strasser & Anselmetti, 2008) and Chile (Moernaut *et al.*, 2007). The major change recognized in the seismic profiles occurs at the transition between seismic units EB and EC, with the first occurrence of interpreted lateral slide deposits. Although we interpret seismic unit EB as representing a proximal proglacial environment, unit EC represents a distal periglacial environment in a basin that was no longer in direct contact with glacial ice, which by that time had retreated towards Cordillera Darwin (Waldmann *et al.*, 2010). Similar seismic architecture has been interpreted from a Holocene succession in former Alpine proglacial lakes (Girardclos *et al.*, 2005).

MASS-WASTING EVENTS IN LAGO FAGNANO

Although the interpreted mass-flow deposits appear in the seismic profiles as wedges of chaotic to transparent seismic facies, with smooth to slightly hummocky top surfaces and erosive bases, the relatively thin, distal parts of these deposits are interpreted as megaturbidites and are characterized by concordant, seismically transparent units that generally overlie undisturbed, acoustically layered sediments (Figs 3 and 4).

© 2010 The Authors
Basin Research © 2010 Blackwell Publishing Ltd, European Association of Geoscientists & Engineers and International Association of Sedimentologists

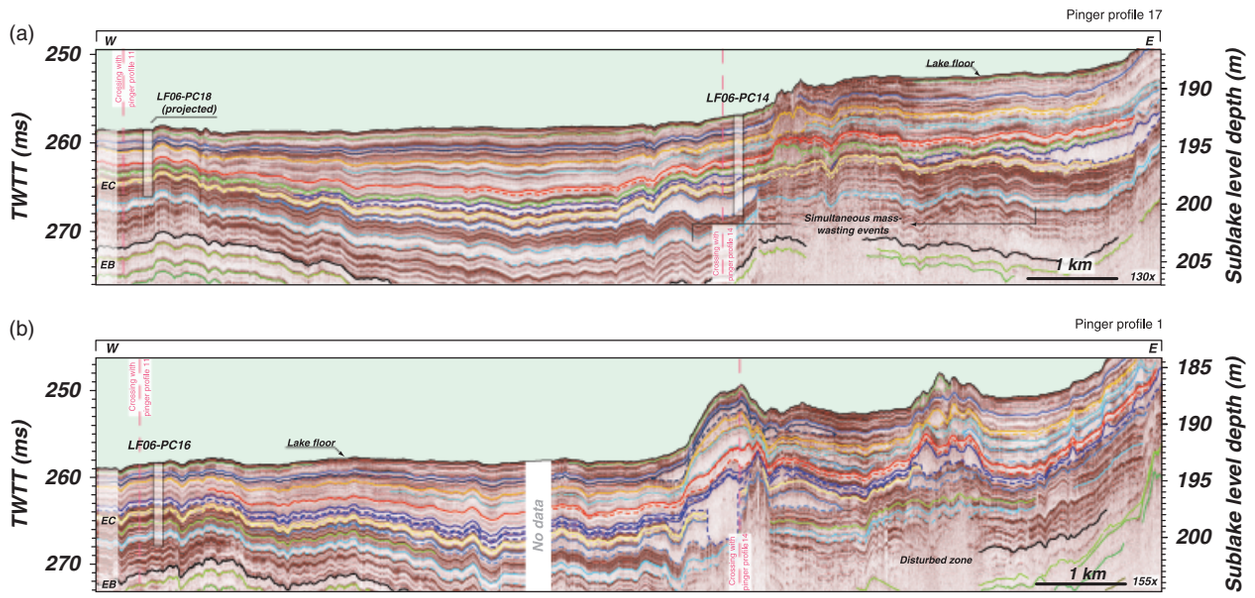

Fig. 4. (a, b) E–W 3.5 kHz sections crossing the entire eastern sub-basin of the lake longitudinally (see Fig. 1d for location). Core positions are labelled. EC and EB represent the different seismic stratigraphic units discussed in the text. Sediment depth is given in milliseconds of two-way traveltime (TWTT), which we convert to sub-lake level depth (m) based on a P-wave velocity of 1430 m s^{-1} for water and 1500 m s^{-1} for sediment. Disturbed zones in the profiles are probably caused by irregular lake floor morphology produced by the buried debris flows. Notice the different vertical exaggeration in both profiles. See legend for the mass-wasting deposit horizons in Fig. 3. For the uninterpreted profiles, the reader is referred to the supplementary material associated with this article.

In this study, the term megaturbidite is used as the distal mass-flow-related units: (i) are thicker than the laminations of the background deposits, (ii) are laterally extensive, (iii) differ in composition from the background sediments, (iv) lack sub-aquatic fan geometries, (v) may consist of a fining upward sequence and (vi) may have an erosional base proximal to the debris flow but do not erode in the basin (Bouma, 1987). On an absolute scale, lacustrine turbidites (e.g. Van Rensbergen *et al.*, 1999; Schnellmann *et al.*, 2005; Fanetti *et al.*, 2008) are at least one order of magnitude smaller compared with their marine counterparts (e.g. Kelts & Hsu, 1980; Siegenthaler *et al.*, 1987). Because large lacustrine turbidite events, however, still represent unique and exceptional events on a basinal scale, we use the term megaturbidites also for these events.

The bases of the mass-flow units in Lago Fagnano subsurface, as marked in the seismic profiles with dashed lines (Figs 3 and 4), represent the lowermost boundary of observed deformation/erosion caused by their downslope movement. As a consequence, these basal boundaries delimit instantaneously emplaced mass-flow deposits, including underlying overridden and deformed sediment, and thus may not represent chronostratigraphic surfaces. In the deeper parts of the eastern sub-basin, the distal parts of these mass-flow deposits, reaching thicknesses of >2 m, pinch out both northward and westward. Both pairs of debris flow and megaturbidite are referred in this paper as generated by a single event and are annotated C1–C24, from the older to the younger mass-wasting deposit, respectively. However, only major recognized event deposits are marked in Fig. 5.

Sedimentology

The sedimentary sequence obtained by coring the deeper parts of the eastern sub-basin of the lake (Fig. 1d) consists of rhythmic intercalations of dark, organic-rich and brown detrital clay laminae, formed in an anoxic or dysoxic sediment/water interface environment, thereby preventing bioturbation (Waldmann *et al.*, 2008). The dark laminae are typified by large diatom content and an increase in Fe and Mn (Figs 5 and 6), perhaps due to periodic increases in productivity related to pulses of humidity arriving from the Pacific Ocean (Waldmann *et al.*, in press). These in turn are likely controlled by fluctuations in the Southern Hemisphere westerly wind belt (Moy *et al.*, 2008). The observed laminated sequence is occasionally interrupted, however, by layers consisting of brown, rather homogenous mud of variable thickness up to 20 cm (Fig. 6). These beds, which we interpret as mass-flow deposits based on their acoustic imaging, internal seismic structure and overall architecture, are scattered in all the cores from this sub-basin at different depths (see Figs 3 and 4).

The so-called Bouma Sequence, originated by turbidity currents in the marine environment (Bouma, 1962), serves as a basic model to compare the internal architecture of megaturbidites in Lago Fagnano and helps to postulate the processes involved in their formation. The Bouma Sequence includes five divisions, namely Ta, Tb, Tc, Td and Te, which are considered to be the product of a single turbidity-current event (Allen *et al.*, 1984). Although Ta is described as a massive graded sand unit, units Tb–Td represent parallel to rippled sand to silt sediments, topped by muddy homogenous clay, the Te unit.

© 2010 The Authors

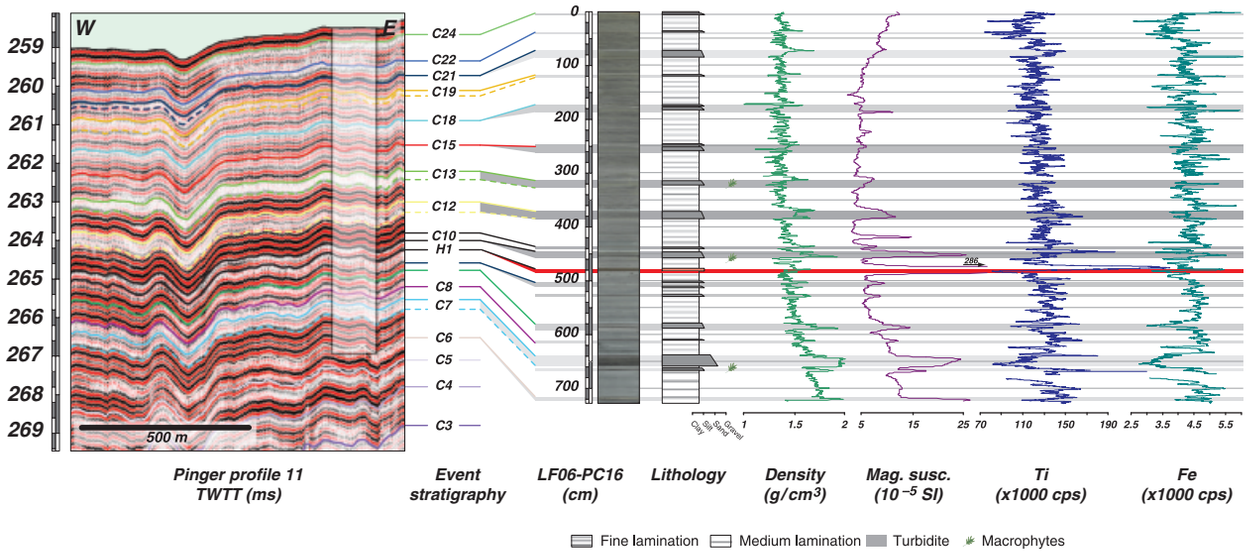

Fig. 5. Correlation between the pinger-11 seismic profile and core LF06-PC16 (see Figs 1d and 3a for locations). This seismic-to-core correlation relates the different mass-flow deposits in the seismic profile to the core. Density and magnetic susceptibility values are higher within interpreted mass-flow layers. Although Fe and Ti increase in the mass-flow layers within the uppermost 5 m (e.g., C21), their values mostly decrease deeper in the core (e.g., C4). These correlations are probably related to different internal mineralogical compositions of the younger and older mass-flow deposits. Red line stands for a tephra level geochemically fingerprinted and lithologically identified as the Hudson H1 event (Stern, 2008; Waldmann *et al.*, in press).

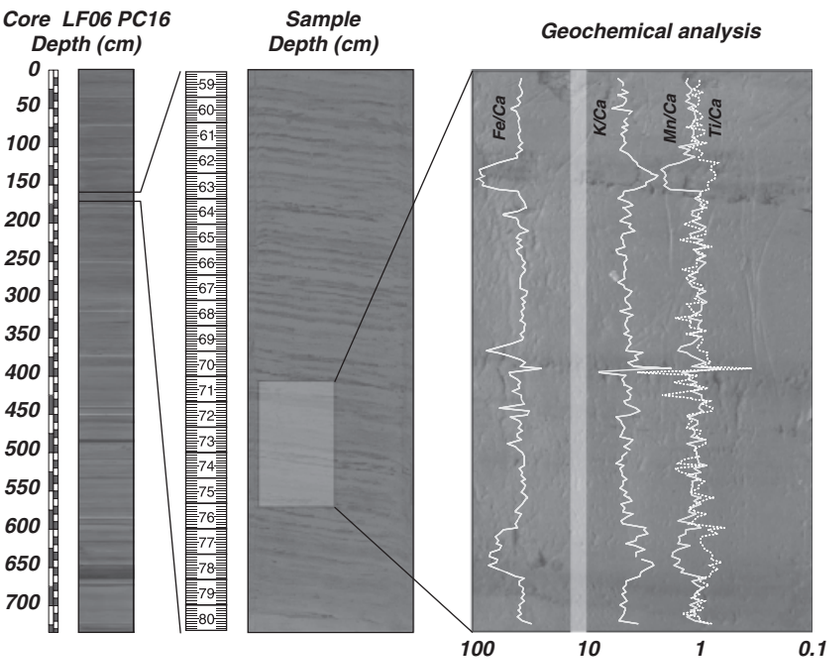

Fig. 6. Core LF06-PC16, with an enlargement of the laminated sequence discussed in the text. Close-up shows the mm-scale lamination in detail (depth in cm). Ultrahigh-resolution X-ray fluorescence analyses of a selected sample (inset box – grey shading indicates sampling location) reveals high Mn/Ca and Fe/Ca ratios in the dark laminae, whereas high Ti/Ca and K/Ca characterize the thicker, lighter laminae. Calcium is used for ratio calculations, since it is a conservative element in the sediments (Waldmann *et al.*, 2008). Dark laminae correlate with high Fe and Mn content, whereas high values of Ti and K correlate with the lighter laminae. See text for further discussion.

Bouma (1962) interprets the Ta unit to represent deposition from a high-density turbidity current, whereas units Tb–Td are inferred as products of traction, or combined traction and suspension. The overlying unit Te is interpreted as the product of pelagic and low-density turbidity currents. Core and outcrop studies have shown that complete and partial Bouma sequences can also be interpreted to be deposits formed by processes other than turbidity currents, for example sandy debris flows and bottom-current reworking (Shanmugam, 1997; Mulder & Alexander, 2001).

In Lago Fagnano megaturbidites, none of the layers show the complete Bouma Sequence, but rather various combinations of these units. The Fagnano mass-flow deposits are characterized by high-density and magnetic-susceptibility values, as well as by an increase in Ti and Fe when compared to background sediment, probably in relation to higher elemental density (counts) for the same lithology (Fig. 5). Moreover, some mass-wasting deposits appear more prominently in the seismic profiles when compared with their cored expression, probably in relation to variations in lithology and density. The Lago Fagnano

© 2010 The Authors
Basin Research © 2010 Blackwell Publishing Ltd, European Association of Geoscientists & Engineers and International Association of Sedimentologists

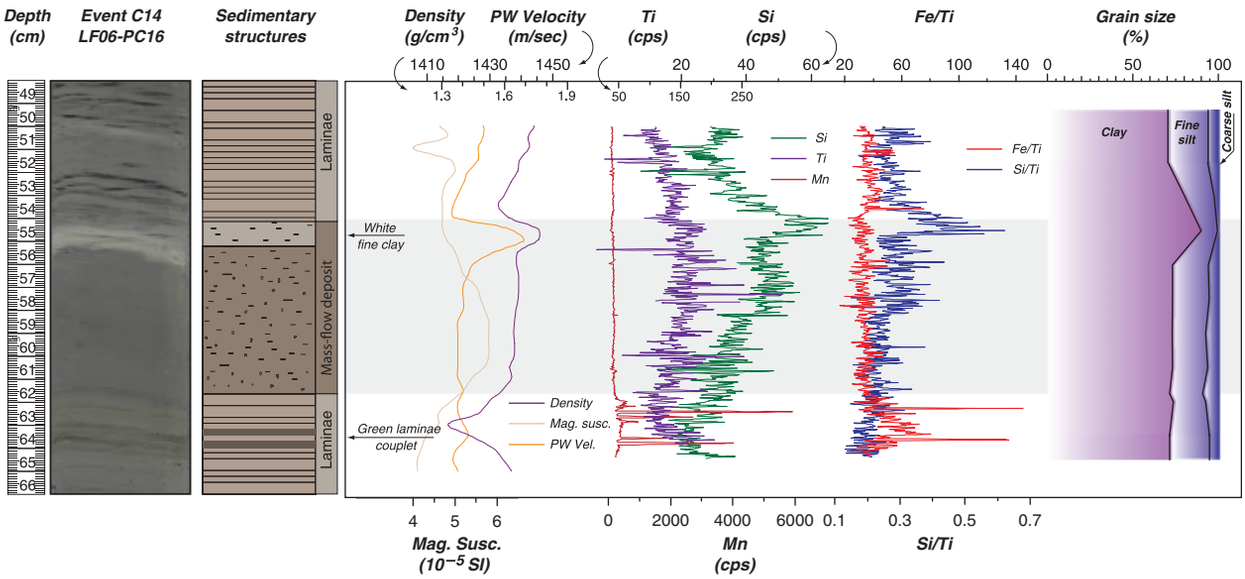

Fig. 7. A cross-section of the C14 distal megaturbidite from core LF06-PC16 (262–254 cm core depth). Close-up shows lithological, petrophysical, geochemical and grain size properties. Cps, counts per second. Note increases of density, P-wave velocity and Si in the upper, white finest-grained part of this deposit. Between core depths of 262 and 255 cm, the interpreted megaturbidite lithology consists of massive homogenous clay with no visible internal structures. A couplet of greenish laminae, probably indicating reducing conditions, is recognized just below the megaturbidite (264–263 cm core depth). Refer to text for a more complete explanation

mass-flow deposits are grouped into three categories considering their thicknesses and internal architecture and may indicate the proximity of the source material: debris flow, thick and thin megaturbidites.

Thin megaturbidite

We have selected one megaturbidite, C14 from core LF06-PC16, to characterize the geochemical, structural and textural variations of these units (Fig. 7). The base of this megaturbidite deposit is a ~6 cm thick, fairly homogenous mud that is capped by 2–3 cm of whitish fine-clay. This megaturbidite is characterized by a generally fining-upward sequence from coarse silt to fine clay at the top. Small wood fragments and plant leaves occur at the base, indicating contribution of allochthonous material or reworked organic matter. Approximately constant petrophysical and geochemical properties typify this and other sampled megaturbidites. However, higher P-wave velocity and density values, as well as higher Si/Ti content, characterize the whitish cap. We attribute changes in these parameters to the compaction of very fine clay deposited by suspension of reworked material occurring during a seiche following emplacement of the deposit (Siegenthaler *et al.*, 1987), and probably to contributions from particles from the epilimnion to the hypolimnion in a layered Lago Fagnano (e.g. Shteinman *et al.*, 1997). Interestingly, two greenish, ~3-mm thick laminae, highly enriched in diatoms and organic matter, occur ~1 cm below the base of this megaturbidite (Fig. 7). Similar laminae, forming couplets, which are also characterized by very low (~1.3 g cm^{-3}) density values and high Fe content, occur below all thin megaturbidites that were cored in the eastern sub-basin. We interpret the occurrence of these greenish laminae as the result of rapid burial and preservation of the contained organic matter in an anoxic environment by rapidly settling overlying mass-wasting deposits. Rapid burial prevented the organic material from decomposing, as it was quickly isolated from dissolved oxygen in the bottom water. This process is also marked by increased values of Mn (Fig. 6) and probably indicates reducing conditions (Koinig *et al.*, 2003). Moreover, the preservation of these two greenish laminae implies that there is no erosion by the megaturbidite in the deeper parts of the lake. We conclude that despite frequent violent depositional events, a total of 24 such events occur in the eastern sub-basin (Figs 3 and 4) in the upper ~8 m of the seismically observed section. The observed basinal sections conserve at least part of a continuous, laminated sedimentary record.

Thick megaturbidite

We chose event C4 to characterize the petrophysical and geochemical variations of a thicker, probably more proximal megaturbidite (Figs 3 and 8). This megaturbidite is 20 cm thick in piston core LF06-PC16 and can be divided into four units (units A–C and W, Fig. 8) on the basis of the internal architecture. Unit A consists of ~7–8 cm thick, graded very-fine to fine sand. A few wood fragments and plant leaves occur at its base, probably indicating contribution of terrestrial material or reworking of previously deposited organic matter. Unit B consists of ~7–8 cm thick, very-fine sand exhibiting graded bedding; faint laminations of finer-grained material also occur. Unit C is composed of a 4–5 cm thick, weakly layered interbedded silt and clay. The sequence A–C is capped by a ~1-cm

© 2010 The Authors

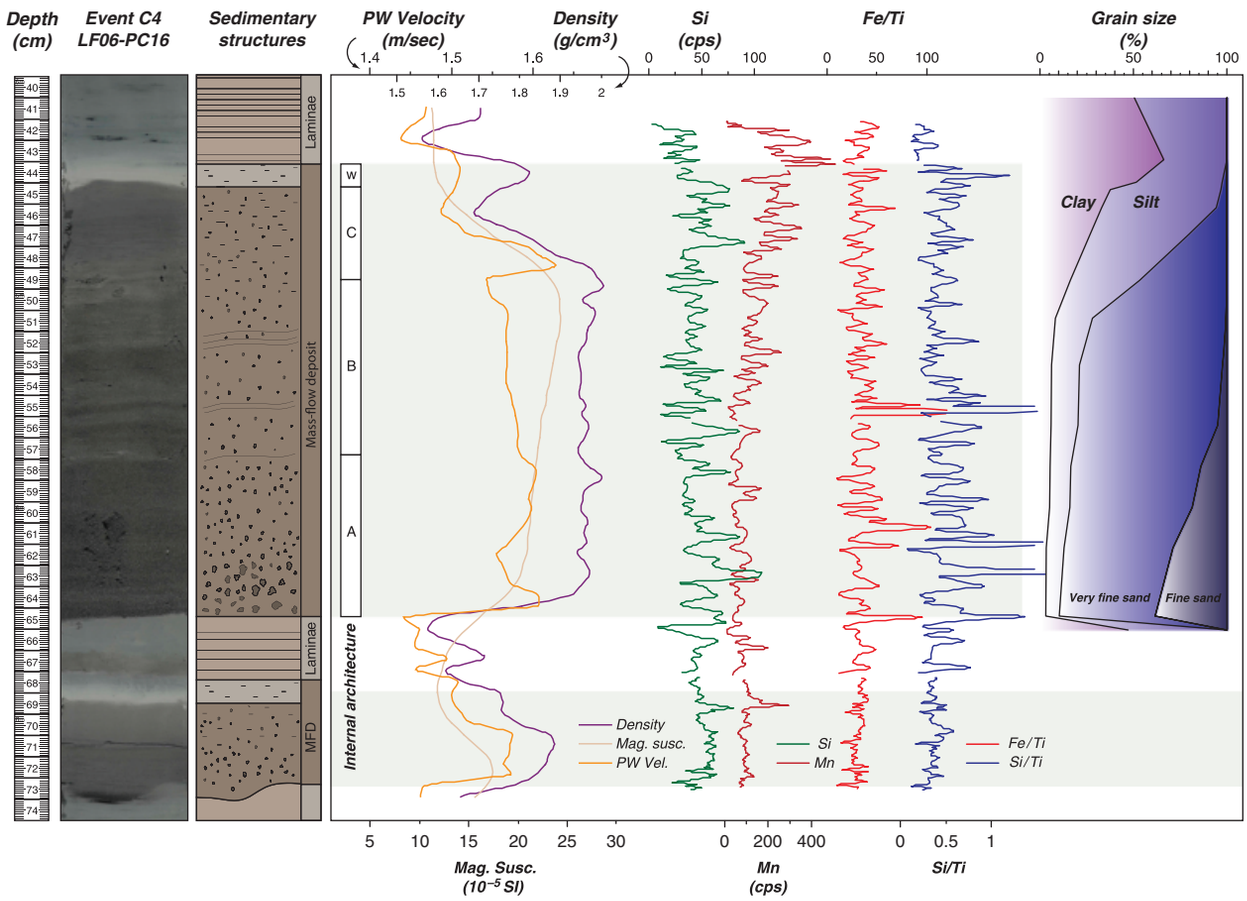

Fig. 8. A core section of event C4, interpreted as a proximal megaturbidite, from piston core LF06-PC16. Close-up shows lithological, petrophysical, geochemical and grain size properties. Cps, counts per second; MFD, mass-flow deposit. Internal units are defined by A, B, C and W (the latter standing for the white cap unit also seen in the interpreted distal megaturbidite of event C14). Density and P-wave velocity increase within units A, B and W, but decrease in unit C. Magnetic susceptibility, however, increases only within units A and B. Geochemical parameters stay relatively stable through the entire megaturbidite, although an increase of Si/Ti is observed in relation to (background) laminated sediments. See text for further comments.

thick, whitish fine-clay (unit W), which is similar to the cap observed in the distal megaturbidite sampled by LF06-PC16 (Fig. 7). The entire sequence fines upward, from fine-sand and silt, to clay at the top. All petrophysical properties increase within C4 in relation to the laminated sediments below and above this deposit (Fig. 8), with higher values than those measured in thin megaturbidites (Fig. 7). However, density and P-wave velocity decrease in unit C of the thick megaturbidite, associated with a grain size reduction from very fine sand to silt. These values increase again in unit W, which is the finest-grained of the units sampled. Magnetic susceptibility values remain relatively constant through units A and B, but decrease in units C and W to values similar to those measured in the laminated (background) deposits above and below C4. In contrast to the distal megaturbidite, geochemical parameters do not exhibit major changes in their values; only Si and Mn slightly increase compared with the encompassing laminated sediments. Furthermore, there is no evidence of the organic-rich green laminae below C4, possibly indicating small amounts of local erosion of basinal sediments by the flow in this more proximal site, even though this erosion must be minor, as it cannot be recognized on the high-resolution seismic data (Fig. 3). The absence of the organic-rich green laminae couplet may indicate as well times of little diatom content in the lake waters or an environment depleted with organic matter. The internal architecture of C4 resembles the divisions described in deposits originated by turbidity currents in the marine environment (Bouma, 1962), probably indicating a similar formation process.

Debris flow

Sampling the most proximal part of one of our seismically interpreted mass-flows, event C9 in core LF06-PC14 (Fig. 3), recovered a highly disturbed mud and silt sequence of 155 cm overlying undisturbed, laminated sediments (Fig. 9). The observed stratigraphic architecture consists of a 4-cm thick light gray clay layer that probably represents a basal shear zone, overlain by a highly folded zone composed by bended layers of light and dark gray clay and silt (~104 cm thick), in turn overlain by a similar deformed zone (~29 cm thick) that includes large (~5 cm)

© 2010 The Authors
Basin Research © 2010 Blackwell Publishing Ltd, European Association of Geoscientists & Engineers and International Association of Sedimentologists

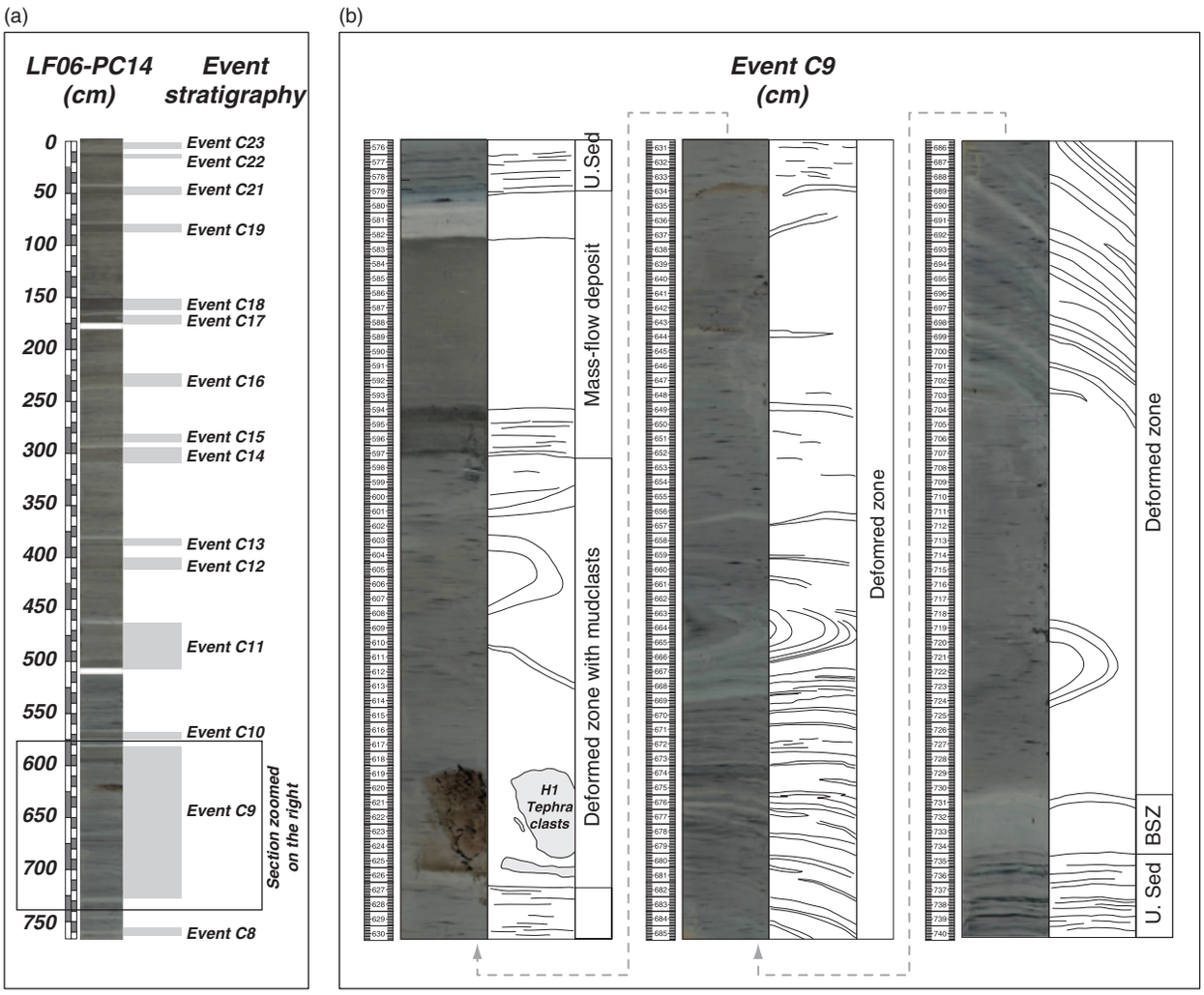

Fig. 9. A core section sampling interpreted debris flow deposit C9. (a) Core LF06-PC14 with the identified mass-flow event stratigraphy. (b) Photograph of the interpreted C9 debris flow from core LF06-PC14. Notice the high degree of deformation of the sediments caused by the mass-flow masses overriding a basal shear zone (BSZ). The upper part of the C9 debris flow (626–597 cm core depth) is characterized by a deformed zone that includes mud- and sand-clasts in a clay matrix. Some of the clasts were identified as material belonging to the Hudson H1 tephra (Stern, 2008). The debris flow is immediately overlain by an ~18 cm thick megaturbidite. *U. Sed*, undisturbed sediments.

mud- and sand-clasts. Clasts of the Hudson H1 tephra have been identified within this uppermost, matrix-supported conglomerate unit. This C9 mud-flow deposit is overlain by an 18 cm thick proximal megaturbidite layer, characterized by a fining upward sequence and capped by a ~3 cm homogenous white clay layer.

The architecture of this debris flow (C9) indicates that the initial slumping was followed by partial disintegration of the source material as it moved downslope. This observation suggests that the debris flow involved rotational sliding of interpreted glacio-lacustrine sediments that covered the uppermost part of the basin escarpment shoulders. The sudden slope break at the edge of the basin would lead to rapid flow deceleration, and, as a consequence, to enhanced sediment deposition in the basin margins further inducing deformation of the overridden sediment package. Previous studies from marine (Piper *et al.*, 1999) and lake (Schnellmann *et al.*, 2005) environments have shown that debris flows can be generated by progressive disintegration of strata within an initial large sub-aqueous landslide. Debris flows formed in this way extend downslope from the landslide, sometimes for large distances, and contain intact blocks and clasts of original landslide material, which includes as well underlying strata. The different sedimentary features and lithological variations occurring during a mass-wasting event are shown in Fig. 10.

SPATIAL AND TEMPORAL DISTRIBUTION OF MASS-MOVEMENT DEPOSITS

We recognize more than nineteen mass-flow deposits (C2–C24 that include debris flow, thick and thin megaturbidites), which we can correlate between cores in the east-

© 2010 The Authors

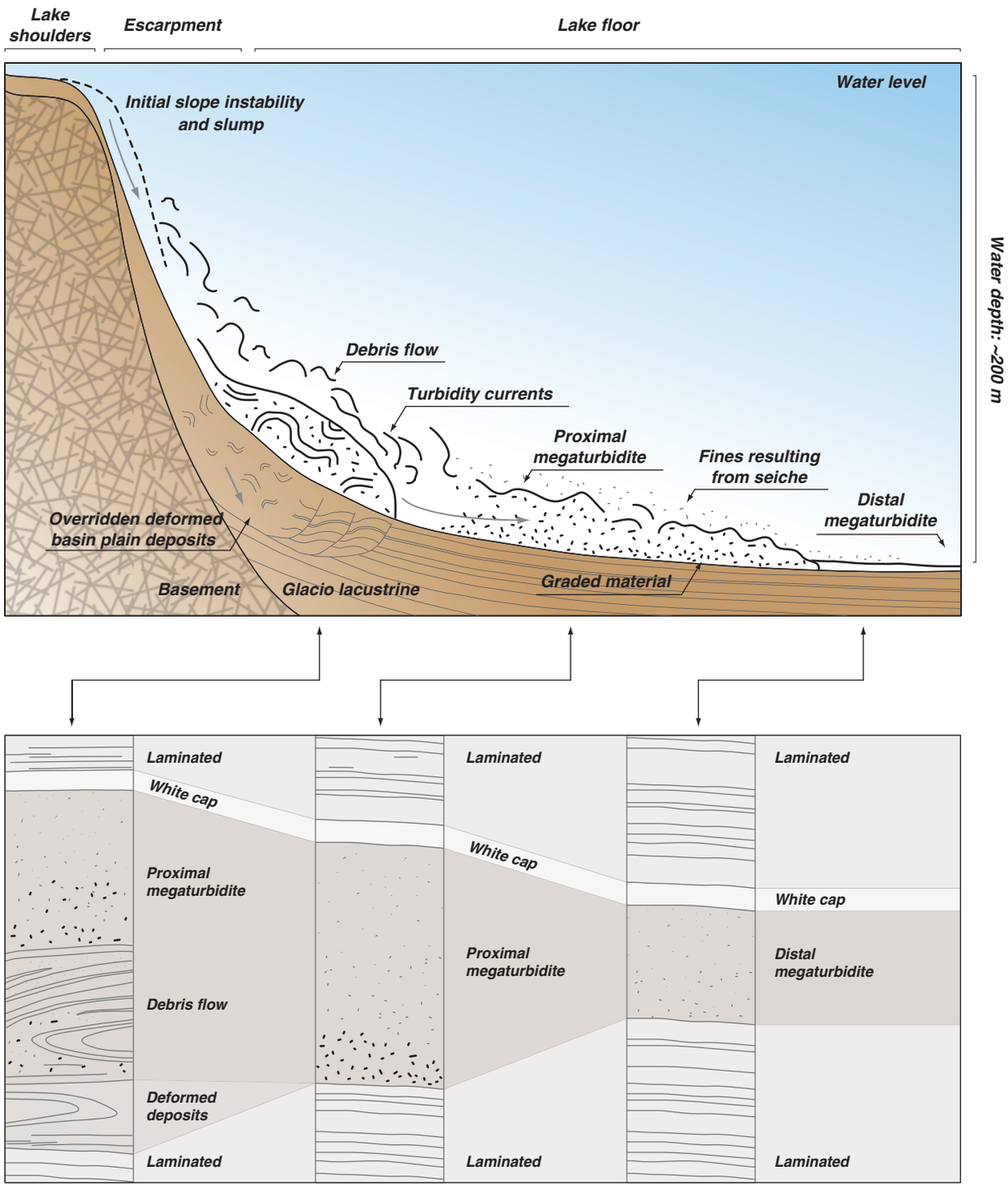

Fig. 10. An illustration representing the sequence of events related to initial slope instability in a lacustrine basin such as Lago Fagnano (above) and the expected cross-section lithology across the mass-flow deposit (below). The descending masses produce slump, rotational sliding and debris flows close to the basin escarpment. As distance increase from the basin wall, and turbidity currents decelerate, the thicknesses of both proximal and distal megaturbidites change accordingly. The clay fraction that rested in suspension slowly deposited forming the white caps that top the mass-wasting deposits.

ern sub-basin of Lago Fagnano (Fig. 11). Events Cl, Cla and Clb were identified in the seismic profiles but not cored (e.g. Fig. 5). Most of the cored mass-flow deposits can be correlated to event horizons that we defined in the seismic profiles (Figs 3 and 4) and their thicknesses vary from 2 to ~150 cm. Thick megaturbidites and debris flow units are much less common in the recovered sedimentary sequences as the selected coring sites are located in the deeper part of the basin and distant from the sediment source. In general, the mass-flow deposits thicken

© 2010 The Authors
Basin Research © 2010 Blackwell Publishing Ltd, European Association of Geoscientists & Engineers and International Association of Sedimentologists

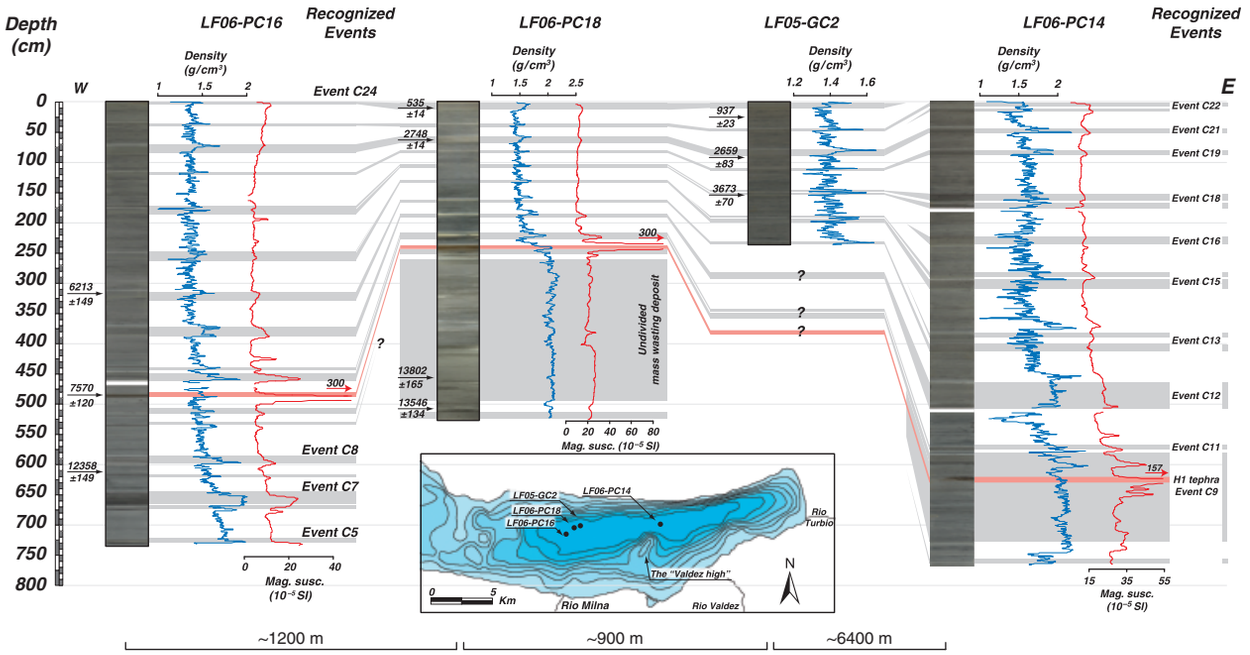

Fig. 11. Event stratigraphy and correlation among sedimentary cores across the easternmost sub-basin of Lago Fagnano. Different megaturbidite deposits are marked by gray shade colours with the respective labels. The Hudson Volcano H1 tephra is highlighted in red. Core locations are shown (inset map. See also Fig. 1d). All ages are years BP, as summarized in Table 1.

eastwards, probably in relation to increased contribution of local source material, while they pond within what was a deeper easternmost part of the sub-basin (Fig. 3; Waldmann *et al.*, 2008). A very prominent tephra layer found in most of the cores (Fig. 11) corresponds to the Hudson H1 volcanic explosion, dated to 7570 ± 120 years BP (Stern, 2008). This tephra layer occurs in place in cores LF06-PC16 and LF06-PC18 but as a reworked clast in core LF06-PC14 and it further assisted to improve the core-to-core correlation. The contrasting depths of the H1 tephra in the cores may suggest as well substantial differences in sedimentation rates. An averaged rate of 0.63 mm yr^{-1} is calculated for core LF06-PC16 when mass-flow deposits are included in the calculation, yet subtracting them reduces the background sedimentation rate to 0.54 mm yr^{-1} for this site.

Physical-property correlations among the different cores reveal detailed patterns in relation to their internal lithology that may provide further hints for possible trigger mechanisms of mass-flow deposits. Although high magnetic susceptibility signatures characterize all bases of mass-wasting deposits, probably in relation to heavy minerals such as magnetite and hematite, high density is characteristic of all white caps (Fig. 11). This relationship follows the same pattern as visualized in the high resolution XRF imagery of the different mass-wasting deposits (Figs 7 and 8). The correlation of these parameters indicates that the signatures integrity, and thus the pattern of coarse fraction deposition, is maintained to some extent through time and distance during the turbidity current. Some density peaks however, appear to be as well related to internal lithological changes of the background laminated sediments and were previously related to changes in the mineralogical composition of the sediments due to precipitation fluctuations in the lake watershed (Waldmann *et al.*, in press).

An age model for the Holocene sedimentary infill of eastern Lago Fagnano has been established by radiocarbon samples and tephrochronology (Waldmann *et al.*, in press). Several ^{14}C ages were obtained from core LF06-PC16 and were compared with data obtained from cores LF05-GC1 and LF06-PC18 (C.M. Moy *et al.*, unpublished data); these dates are summarized in Table 1. Unfortunately, potential contamination by old or 'dead' carbon sources within the watershed and/or by remobilization and deposition of older lacustrine sediments is possible, so we treat these ages as maximum for their corresponding stratigraphic levels. The age model presented here is defined best for core LF06-PC16 (Fig. 12), which covers both the laminated background sedimentary record and the mass-wasting events C2–C24. The calculated ages of the different mass-wasting events are listed in Table 2.

On the basis of the age model obtained in core LF06-PC16, and the observed spatial and temporal distribution of mass-flow deposits, we propose an event chronology comprising the major mass-wasting deposits within uppermost seismic unit EC (Fig. 3) of the easternmost sub-basin during the Holocene (Fig. 13). Only major events C4, C9, C12, C14, C15, C17 and C19 are included, leaving unmapped minor event horizons, e.g., mass-flow deposits with thicknesses < 5 cm. We can only construct isopach maps of deposits where seismic and core coverage exists. Only interpreted mass-flows of the Holocene were mapped, whereas older deposits deeper than unit EC were not included.

We highlight three important points (Fig. 13):

© 2010 The Authors

Table 1. Isotope data, radiocarbon and calibrated ages retrieved from the cores in the eastern lake sub-basin

Core	Sample	Depth (cm)	Material	^{14}C age (years BP)	^{13}C (‰)	Cal. age (years BP)
LF06-PC18	PC18-4-10	10	Terrestrial macro	505 ± 35	− 26	535 ± 14
	PC18-4-61.5	61.5	Terrestrial macro	2610 ± 35	− 26	2748 ± 14
	PC18-1-60.5	457	Terrestrial macro	11 890 ± 90	− 26	13 802 ± 165
	PC18-1-110	506.5	Terrestrial macro	11 660 ± 50	− 26	13 546 ± 134
LF05-GC2	LF01-22	15	Pollen	1015 ± 35	− 27	937 ± 23
	LF01-91	80	Pollen	2565 ± 35	− 27	2659 ± 83
	LF01-153	185	Terrestrial macro	3410 ± 50	− 27	3673 ± 70
LF06-PC16	PC16-T1	480	Tephra	6850 ± 150	NA	7570 ± 120
	PC16-C15	318	Wood	5445 ± 125	− 20.3	6213 ± 149
	PC16-C23	612	Wood	10 435 ± 75	− 28.4	12 358 ± 149

Tephra age obtained from Stern (2008). Ages for LF05-GC2 are extrapolated from twin core LF05-GC1 (C.M. Moy *et al.*, unpublished data). Calibration was calculated using the web-based CalPal share-ware converter tool (Weninger *et al.*, 2009).

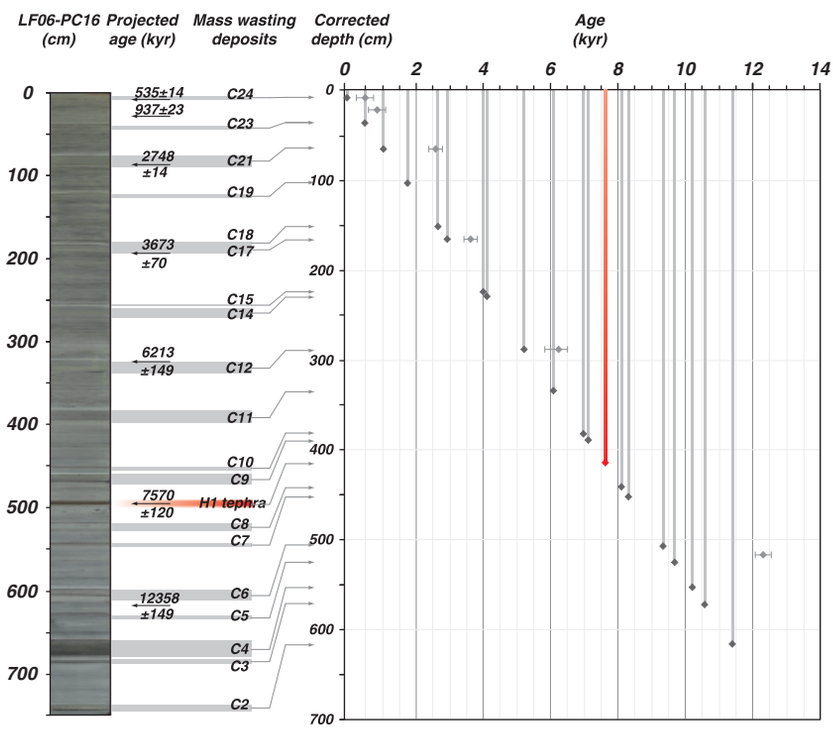

Fig. 12. Corrected depth–age relationship and event stratigraphy of core LF06-PC16 considering a constant background sedimentation rate of 0.54 mm yr^{-1} and the mass-flow deposits thicknesses removal. Projected ages of both radiocarbon and the H1 tephra are shown as well on the right of the core. Red bar stands for the Hudson Volcano H1 tephra level. Grey diamonds with corresponding error bars stand for the projected age.

(a) The elongated E–W geometry of the lake's eastern sub-basin likely defines the direction of mobility and transportation of suspended material. Debris flows are thickest mostly close to the lake's southern slopes (see Fig. 3, pinger profile 14) where the descending sediment masses initially accumulate and deformation of overridden basin sediment is strongest. In contrast, interpreted megaturbidite deposits extend for several tens of kilometres, often covering the entire basin floor (see Fig. 10).

(b) Multiple mass-wasting events appear to occur simultaneously in different parts of the eastern sub-basin. For example, four such events occur at ∼5240 years BP during event C12 and four events occur as well during the C17 event, ∼3980 years BP (Fig. 13d and g, respectively).

(c) Locations of slope instabilities are controlled by moderately steep lateral slopes (> 30–40°), which permit accumulation of unstable lake sediments prone to sliding. Previous seismic stratigraphic analyzes of the deeper part of the lake (Waldmann *et al.*, 2010) reveal that the 'Valdez high' (see Fig. 13a for location) is an inherited morphological structure related to the presence of a ∼50 m thick submerged moraine in the subsurface, which provides ideal lateral slopes on which sediments can accumulate, consequently charging the slope. Thicknesses of most of the mass-wasting deposits increase toward this structure and the southern shores of the lake, where a gentler slope permits sediment accumulation. The northern slopes appear too steep to accumulate sediments; yet some mass-wasting deposits of sub-aquatic origin were triggered

© 2010 The Authors
Basin Research © 2010 Blackwell Publishing Ltd, European Association of Geoscientists & Engineers and International Association of Sedimentologists

Table 2. Reconstructed chronology of the different mass-flow deposits as recognized in seismic unit EC

Event	Depth (cm)*	Thickness (cm)†	Accumulated thickness (cm)‡	Corrected depth (cm)§	Calculated (years BP)¶	Recurrence interval‖
C24	10	2	2	8	56	518
C23	40	2	4	36	574	537
C21	80	11	15	65	1111	703
C19	120	2	17	103	1814	888
C18	170	2	19	151	2702	278
C17	190	5	24	166	2980	1073
C15	250	2	26	224	4053	93
C14	262	7	33	229	4146	1092
C12	330	9	42	288	5238	851
C11	390	14	56	334	6089	888
C10	442	4	60	382	6978	130
C9	460	11	71	389	7107	962
H1	*490*	*5*	*76*	*414*	*7570*	*Tephra*
C8	520	3	79	441	8070	204
C7	535	4	83	452	8273	1018
C6	600	10	93	507	9291	333
C5	620	2	95	525	9624	518
C4	670	22	117	553	10 143	352
C3	695	6	123	572	10 494	814
C2	748	9	132	616	11 309	625

Sedimentation rate (mm year^{-1}): 0, 54

Numbers in italics stand for values of the tephra layer.
*Depth of the mass-flow deposits.
†Thickness of each mass-flow deposit layer (in cm).
‡Accumulated thickness of the mass-flow deposits (in cm).
§Corrected depth of the background sediments excluding the different mass-flow deposits (in cm).
¶Calculated age (in years BP) taking into consideration the Hudson H1 tephra, radiocarbon ages and background sedimentation rate of 0.54 mm year^{-1}.
‖Calculated recurrence interval of each consecutive pair of mass-flow deposits considering the calculated age of each event and constant background sedimentation rate during all the time interval.

there and may indicate the existence of slope instability in this region as well.

POSSIBLE TRIGGERING MECHANISMS OF MASS-WASTING EVENTS

Megaturbidite deposits have been referred to in various geologic settings as homogenites (Kastens & Cita, 1981; Chapron *et al.*, 1999) and seismoturbidites (Nakajima & Kanai, 2000; Shiki *et al.*, 2000) in an attempt to identify their nature. In the case of Lago Fagnano, these distal units consist of redeposited sediments that became suspended in the water column during the slumping/sliding and associated tsunami and seiche action in a small/closed basin. The reconstructed record of slope failure, remobilization and sedimentary transport processes in eastern Lago Fagnano allowed us to evaluate their long-term causes and short-term triggering mechanisms.

Mass movements can be triggered by several processes, such as slope-sediment overloading, substantial lake level variations, extreme flood events, delta collapses and seismicity (Siegenthaler & Sturm, 1991). Nevertheless, documenting synchronicity of multiple features (Ettensohn *et al.*, 2002; Schnellmann *et al.*, 2002) and identifying initial slope sediment stability (Strasser *et al.*, 2007) are generally considered the keys to inferring a regional seismic triggering mechanism. The lateral slopes of the Fagnano eastern sub-basin consist of fine-grained lacustrine lithologies (C.M. Moy *et al.*, unpublished data) and are indeed statically stable. Therefore, nucleating their instability and further mobilization requires additional dynamic loading (i.e. seismic shake) with minimal intensities of ~VII (Monecke *et al.*, 2006; Strasser *et al.*, 2006, 2007). In contrast, delta collapses may occur as well aseismically, but in these cases, down-going sediments are dominated by sandy lithologies, which coring results in Lago Fagnano prove not to be the case (Fig. 5). Furthermore, the effect of lake level changes on slope instability is considered in the case of Lago Fagnano to be minimal, as the source areas of the mass-flows are not in shallow water. In addition, overall lake level fluctuations of Lago Fagnano during the Late Glacial and Holocene, controlled by outflow elevation and to some degree by runoff, are believed to be rather small when compared to water depth of the sediment-charged slopes and the basin. Hyperpycnal flows generated by floods may have produced megaturbidites as well, yet their internal architecture (coarsening-upward unit underlying a fining-upward layer; St-Onge *et al.*, 2004) differ from those typifying Lago Fagnano sediments. Moreover, the different mass-flow deposits

© 2010 The Authors

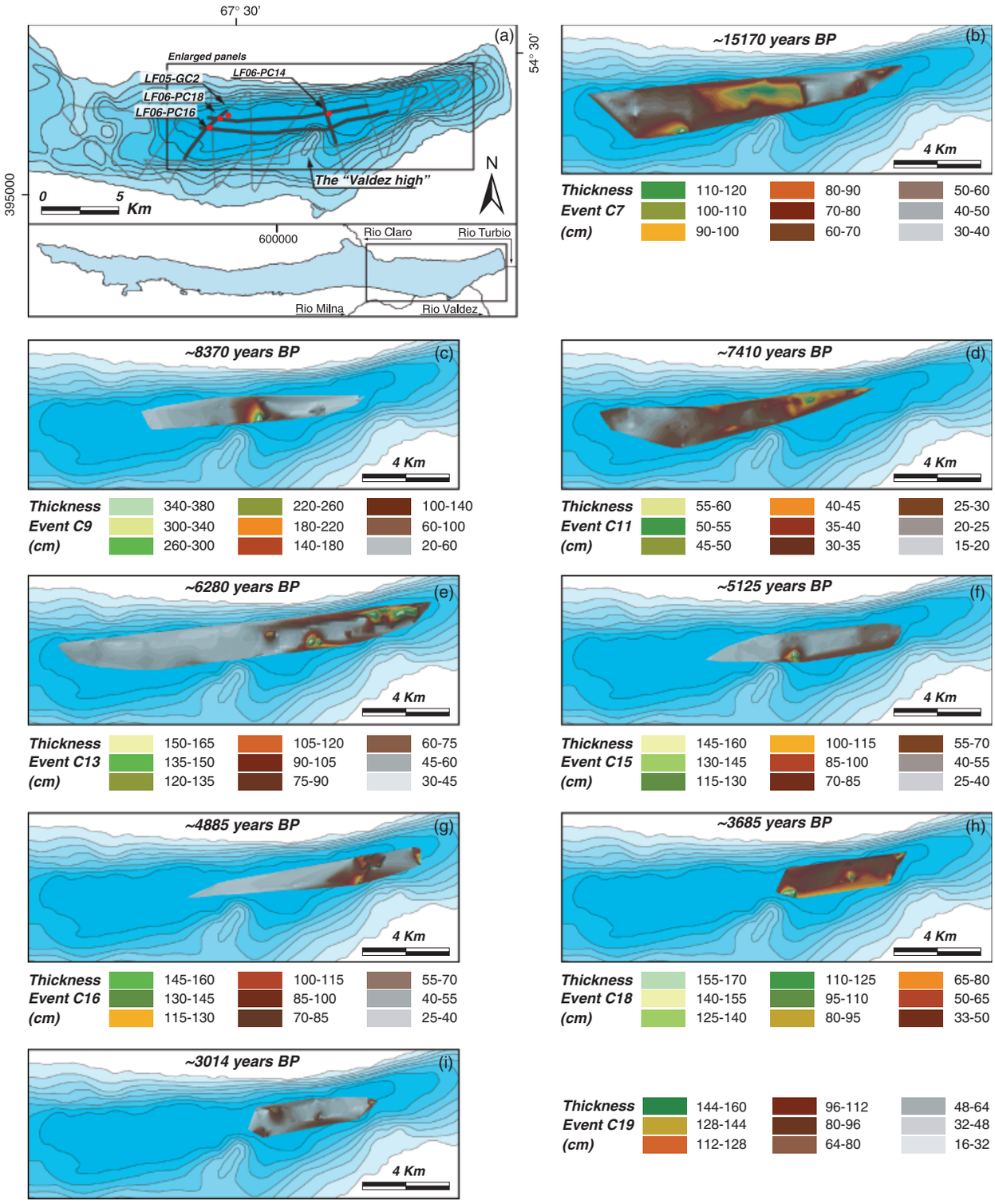

Fig. 13. (a) Location map of the eastern sub-basin. The seismic profile grid is marked by grey lines, and red dots stand for the cores which were used for mapping and core correlation presented in Fig. 5. Main rivers entering the eastern sub-basin are marked in the map inlet. (b–h) Isopach maps of selected mass-flow deposits in the subsurface of Lago Fagnano. Each panel represents different events and has its own coloured legend. Thicknesses are in cm and calculated ages in years BP. Panels b, d, f, g and h show multiple mass-wasting events.

thicken independently from the locations of the main river mouths entering the eastern sub-basin (Fig. 13a), thus reinforcing our assumption for possible seismic triggering.

In conclusion, the combination of seismic and core data with detailed sedimentological analyzes support a mainly seismic triggering mechanism for the different mass-wasting deposits. We thus propose three possible mechanisms

© 2010 The Authors
Basin Research © 2010 Blackwell Publishing Ltd, European Association of Geoscientists & Engineers and International Association of Sedimentologists

for regional seismic triggering: (a) the Magallanes-Fagnano transform, (b) isostatic rebound and (c) the Chile subduction zone.

The Magallanes-Fagnano transform

The last historically recorded large earthquake along the MFT fault zone occurred in 1949, with a magnitude of $M_w = 7.8$ (Lomnitz, 1970). Despite the fact that this large earthquake was destructive, affecting large regions in Tierra del Fuego (Menichetti *et al.*, 2001), it is uncertain what the extent of slope failure was in Lago Fagnano. It is expected however, that an event of such magnitude would dominate the shallow sedimentary record. The youngest mass-wasting deposit (C24) may have resulted from this shaking event (Fig. 12), although radionuclide dating (e.g. ^{210}Pb and ^{137}Cs) of the uppermost part of the sedimentary record have been unsuccessful so far in identifying this historical earthquake and further sampling is needed.

We assume that the sensitivity of Lago Fagnano sediments to MFT seismicity increased after the Fagnano glacier completely retreated from the basin (Waldmann *et al.*, 2010), because initiation of hemipelagic type sedimentation in the slopes may have provided adequate material for subsequent slope failure during shaking. Gravitational collapses of over-steepened deltas carrying silt-laden glacial meltwaters during quake shaking may have provided as well remobilized material to the deep basinal areas, yet their proper identification within the older seismic stratigraphic record is unclear. Correlation to other regional recorders of paleoseismicity, such as marine cores or active fault scarps, may further improve our proposed age model and refine the event catalogue, but those data are not yet fully available (see Lodolo *et al.*, 2003). Moreover, empirical equations involving similar studies of sediment deformation structures in cores obtained along the entire MFT fault zone length [e.g. marine cores east of South America (Fig. 1b), lake cores in the western sub-basin of Lago Fagnano (Fig. 1c)], constrained by high-quality age models, should improve our understanding of the intensity, magnitude and locations of past earthquake epicentres in this increasingly populated region of South America.

Isostatic rebound

Individual mass-wasting deposits in Lago Fagnano may also have been triggered by earthquake activity associated with post-glacial isostatic rebound of the Fuegian Andes, similarly to alpine lakes (Beck *et al.*, 1996). Isostatic uplift rates calculated from dated shells obtained from elevated beaches along the Atlantic Ocean coast and in the Beagle Channel are 0.09 and 2.9 mm yr^{-1}, respectively (Gordillo *et al.*, 1992, 1993; Bujalesky *et al.*, 1997). These calculated rates clearly increase westward, where the thickness of the Cordillera Darwin ice cap during the LGM was the greatest (Fig. 1b; Coronato *et al.*, 2009). A similar mechanism involving increased sediment load following deglaciation has been invoked to justify a series of mass-wasting deposits off Western Wilkes Land in East Antarctica (Donda *et al.*, 2008). Moreover, significant rapid lake level changes following deglaciation may have also influenced local seismicity, such as drainage of dammed lakes (McCulloch *et al.*, 2005), therefore increasing the probability for triggering mass-wasting deposits in Lago Fagnano.

Glacioisostatic uplift may have attained its highest rate immediately following ice retreat, slowly decreasing within a few thousand years, as is well recorded in the North Sea and adjacent areas (Nesje & Sejrup, 1988). Indeed, the recurrence interval of mass-wasting events, as imprinted in Lago Fagnano sediments, appears to have increased between ~11 and 7 ka (Fig. 12). Yet, considering the current dataset, it is not possible to determine which mass-wasting deposit was triggered by isostatic rebound or by seismicity along the MFT during this time interval, even though plate boundary movements are generally expected to cause larger and more frequent seismic events.

The Chile subduction zone

High convergence rates (~80 mm yr^{-1}; DeMets *et al.*, 1990) and very strong earthquakes (e.g. the 1960, $M_w = 9.5$ Valdivia earthquake) typify the Chile subduction zone north of the Chile Triple Junction (CTJ; Fig. 1a for location). In contrast, seismicity south of the CTJ region has been relatively low, with convergence rates as low as 20 mm yr^{-1} (Behrmann & Kopf, 2001). Moreover, the subduction zone south of the CTJ is characterized by a low thermal gradient, as well as by a paucity of shallow earthquake activity between the trench axis and the coastal mountain ranges (Oleskevich *et al.*, 1999). Furthermore, earthquake clustering at the latitude of the Fuegian archipelago decreases eastwards, with increased distance from the subduction front. Therefore, we suggest that seismicity along the Chile subduction zone has not triggered mass-wasting deposits in Lago Fagnano. Instead, recurring proximal paleoseismicity of the MFT seems to be the key trigger of these events.

EARTHQUAKE RECURRENCES

Studies of earthquake recurrences are crucial to assess seismic hazard. The recurrence interval of strong earthquakes ($M_w \geq$ ~7) in areas with high deformation rates, such as interplate regions, is high: e.g., few hundreds to 1000 years for the Dead Sea transform (Migowski *et al.*, 2004; Begin *et al.*, 2005), ~480 years for the North Anatolian fault (Ambraseys & Finkel, 1991; Beck *et al.*, 2007), and ~100–230 years for the San Andreas fault (Wallace, 1970; Parsons *et al.*, 2006; Goldfinger *et al.*, 2007). The time span covered by historical records in Lago Fagnano is short, due to only recent documented human settlement in this region. Nonetheless, the temporal and spatial continuity of Lago Fagnano sediments provide a high-resolution archive of slope failure and debris flow/megaturbidite formation probably in relation to large prehistoric seismic events.

© 2010 The Authors

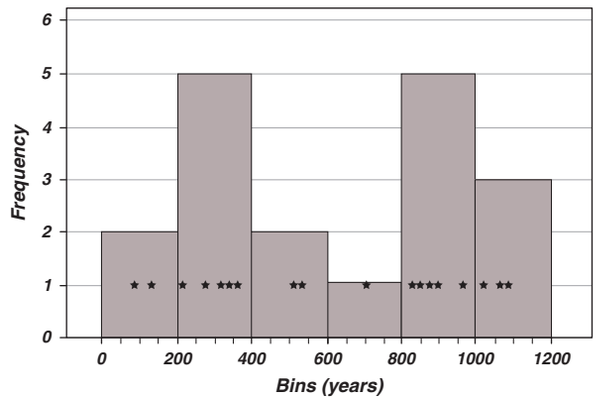

Fig. 14. Histogram showing the number of major mass-flow events ($n = 19$) within 200-year bin (brown bars). The recurrence intervals between each pair of adjacent events are denoted by black stars. The majority of recurrence intervals occur between ~100 and ~1100 years, with two clusters around ~350 and ~850 years. Calculated ages of the different mass-wasting events are extrapolated from Table 2.

The 19 major mass-flow sequences (with thicknesses > 5 cm comprising C2–C24; Fig. 12) identified within the eastern sub-basin sedimentary package of Lago Fagnano provide a robust database of seismic activity during the Holocene. With a long paleoseismic record we can draw some preliminary conclusions about the distribution of recurrence intervals with time. A frequency histogram in 200-year intervals is reconstructed for these events estimating intensities > ~VII (Fig. 14). While preliminary, this suggests that the majority of repeated intervals lie between ~100 and ~1100 years, with two clusters of events around ~350 and ~850 years.

If we consider the MFT fault zone to be the main generator of seismicity, and despite uncertainties of earthquake dates, the data presented here offer new insights into seismic activity in Tierra del Fuego through time. We speculate that the interval between the end of one temporal cluster and the next, might best be termed as a 'supercycle', because most often the cycle terminates in two events rather than just one single large earthquake (Fig. 12), as it was identified at some extent as well in the San Andreas fault system (Jacoby *et al.*, 1988; Grant & Sieh, 1994). The bimodal recurrence of large earthquakes as identified in the Lago Fagnano record may represent as well rupture of different portions of the MFT fault or incomplete strain release along the transform fault during large earthquakes. Moreover, isostatic rebound following deglaciation of the Fuegian ice cap may have enhanced seismic activity shortening the recurrence interval of earthquakes in the region.

CONCLUSIONS

Combining basin-wide high-resolution seismic surveys with sediment core analysis from the subsurface of eastern Lago Fagnano allows identification and dating of Holocene mass-wasting deposits. The following points summarize the results from this study:

1. Lateral sliding in Lago Fagnano has induced the formation of debris flows accumulating close to the basin slope and directly linked proximal/distal megaturbidites covering large parts of the eastern sub-basin.
2. More than 19 mass-wasting deposits were recognized in the seismic stratigraphy and cored sediments from the eastern sub-basin of Lago Fagnano. Thicknesses of basinal megaturbidites range between 5 and 50 cm, consisting of fairly homogenous brownish mud fining upward from fine sand-silt to clay. The sequences are generally capped by a 2–3 cm thick, whitish clay bed that we interpret as deposition of the finest suspended fraction after the event, possibly also related to seiche/tsunami movements of lake waters in response to seismic shaking.
3. Some low-density, diatom-enriched greenish laminae (usually couplets) are well preserved immediately below each megaturbidite. This lithology indicates rapid burial of lacustrine organic matter by the deposition of these megaturbidites in a non-erosive and non-destructive fashion, allowing its preservation in an anoxic pore-water environment.
4. Slope failure may occur synchronously in several parts of the eastern lake basin, suggesting that earthquakes as most likely triggering mechanism for their formation.
5. The age model for the major mass-wasting events is based on radiocarbon dating and tephrochronology and spans the entire Holocene. It suggests an average seismic recurrence interval, likely along the MFT system, of ~350 and ~850 years, which is comparable to similar transforms elsewhere. Yet, earthquake triggering by isostatic rebound caused by deglaciation of the Fuegian Andes cannot be neglected, considering possible clustering of events between ~11 and 7 kyrs. We estimate that seismicity triggered along the subduction zone south of the CTJ is unlikely to produce mass-flow deposits in Lago Fagnano, as these quakes are too far west and of small intensity to destabilize the lake sediments.
6. An improved chronology of Lago Fagnano sediments and comparing this event stratigraphy record with other archives along the MFT (both continental and marine), could serve as a basis for reconstructing epicentre locations and earthquake magnitudes for this region in the past. Nevertheless, the results of this study represent the first quantitative estimate of recurring earthquake hazard in Tierra del Fuego.

ACKNOWLEDGEMENTS

We wish to thank Steffen Saustrup and Mark Wiederspahn of the Institute for Geophysics, and David Mucciarone of Stanford, for technical assistance during all aspects of the fieldwork. Stanford University (Dunbar) supplied the *R/V Neecho*. This work further benefited from constructive

© 2010 The Authors
Basin Research © 2010 Blackwell Publishing Ltd, European Association of Geoscientists & Engineers and International Association of Sedimentologists

discussions with Michael Strasser (University of Bremen), Stephanie Girardclos (University of Geneva), Christine Zühlsdorff (University of Bergen) and Emmanuel Chapron (University of Orleans). The logistical help and hospitality of Alejandro, Maria Elena and Gabriel Echeverría from Bahía Torito on Lago Fagnano are kindly acknowledged. Centro Austral de Investigaciones Científicas (CADIC) at Ushuaia supplied housing and logistical support during the field seasons. This work is part of the project Environmental Changes Down-South (ENDS) supported by the Swiss National Science Foundation, grants 200021-100668/1 and 200020-111928/1 (to Ariztegui and Anselmetti). We also acknowledge support from the U.S. National Science Foundation (to Dunbar) and the National Geographic Society (CRE grant 7705-04 to Austin). We also thank two anonymous reviewers and Marc De Batist for critical comments that significantly improved the manuscript. This is UTIG Contribution Number 2273.

SUPPORTING INFORMATION

Additional Supporting Information may be found in the online version of this article:

Figure S1. Un-interpreted (left) and interpreted (right) SW-NE (a) and N-S (b) 3.5 kHz sections crossing the eastern sub-basin (location of profiles in Fig. 1). Positions of cores are also labeled. EC and EB in the lower figure represent the different seismic units. Sediment depth is given in milliseconds of two-way traveltime (TWTT). We convert these travel-times to sub-lake level depth (m) based on a P-wave velocity of 1430 m s^{-1} for water and 1500 m s^{-1} for sediment. The different color horizons stand for the different mass-wasting deposits. Notice the different vertical exaggeration in both profiles.

Figure S2. a) and b) un-interpreted (above) and interpreted (below) E-W 3.5 kHz sections crossing the entire eastern sub-basin of the lake longitudinally (see Fig. ld in the main article for location). Core positions are labeled. EC and EB represent the different seismic stratigraphic units. Sediment depth is given in milliseconds of two-way traveltime (TWTT), which we convert to sub-lake level depth (m) based on a P-wave velocity of 1430 m s^{-1} for water and 1500 m s^{-1} for sediment. Notice the different vertical exaggeration in both profiles. See legend for the mass-wasting deposit horizons in Fig. 1 of supplementary material.

Please note: Wiley-Blackwell are not responsible for the content or functionality of any supporting materials supplied by the authors. Any queries (other than missing material) should be directed to the corresponding author for the article.

REFERENCES

Allen, C.R., Gillespie, A.R., Han, Y.A., Sieh, K.E., Zhang, B.C. & Zhu, C.N. (1984) Red river and associated faults, Yunnan province, China – Quaternary geology, slip rates, and seismic hazard. *Geol. Soc. Am. Bull.*, **95**, 686–700.

Ambraseys, N.N. & Finkel, C.F. (1991) Long-term seismicity of Istanbul and of the Marmara sea region. *Terra Nova*, **3**, 527–539.

Beck, C., Manalt, F., Chapron, E., Van Rensbergen, P. & De Batist, M. (1996) Enhanced seismicity in the early post-glacial period: evidence from the post-würm sediments of Lake Annecy, Northwestern Alps. *J. Geodyn.*, **22**, 155–171.

Beck, C., Mercier de Lepinay, B., Schneider, J.-L., Cremer, M., Cagatay, N., Wendenbaum, E., Boutareaud, S. & Menot, G. (2007) Late quaternary co-seismic sedimentation in the sea of Marmara's deep basins. *Sediment. Geol.*, **199**, 65–89.

Begin, Z.B., Steinberg, D.M., Ichinose, G.A. & Marco, S. (2005) A 40,000 year unchanging seismic regime in the dead sea rift. *Geology*, **33**, 257–260.

Behrmann, J.H. & Kopf, A. (2001) Balance of tectonically accreted and subducted sediment at the Chile triple junction. *Int. J. Earth Sci.*, **90**, 753–768.

Bookman, R., Driscoll, C.T., Engstrom, D.R. & Effler, S.W. (2008) Local to regional emission sources affecting mercury fluxes to New York lakes. *Atmos. Environ.*, **42**, 6088–6097.

Bouma, A. (1962) *Sedimentology of Some Flysch Deposits: A Graphic Approach to Facies Interpretation*. Elsevier, Amsterdam.

Bouma, A. (1987) Megaturbidite: an acceptable term? *Geo-Mar. Lett.*, **7**, 63–67. doi: 10.1007/BF02237985.

Bujalesky, G.G., Heusser, C.J., Coronato, A.M., Roig, C.E. & Rabassa, J.O. (1997) Pleistocene Glaciolacustrine sedimentation at Lago Fagnano, Andes of Tierra Del Fuego, Southernmost South America. *Quat. Sci. Rev.*, **16**, 767–778.

Chapron, E., Beck, C., Pourchet, M. & Deconinck, J.F. (1999) 1822 earthquake-triggered Homogenite in Lake Le Bourget (Nw Alps). *Terra Nova*, **11**, 86–92.

Chapron, E., Van Rensbergen, P., Beck, C., De Batist, M. & Paillet, A. (1996) Lacustrine sedimentary record of Brutal events in Lake Le Bourget (Northwestern Alps-Southern Jura). *Quaternaire*, **7**, 155–168.

Coronato, A., Seppälä, M., Ponce, F. & Rabassa, J. (2009) Glacial geomorphology of the Pleistocene Lake Fagnano Ice Lobe, Tierra Del Fuego, Southern South America: alpine and lowland glacial landscape. *Geomorphology*, **112**, 67–81.

Costa, C.H., Smalley, J.R., Schwartz, D.P., Stenner, H.D., Ellis, M., Ahumada, E.A. & Velasco, M.A. (2006) Paleoseismic observations of an onshore transform boundary: the Magallanes-Fagnano fault, Tierra Del Fuego, Argentina. *Rev. Asoc. Geol. Argentina*, **61**, 647–657.

Cunningham, W.D. (1993) Strike-slip faults in the Southernmost Andes and the development of the Patagonian Orocline. *Tectonics*, **12**, 169–186.

DeMets, C.R., Gordon, R.G., Argus, D. & Stein, S. (1990) Current plate motions. *Geophys. J. Int.*, **101**, 425–478.

Donda, F., O'Brien, P.E., De Santis, L., Rebesco, M. & Brancolini, G. (2008) Mass wasting processes in the Western Wilkes land margin: possible implications for East Antarctic glacial history. *Palaeogeogr. Palaeoclimatol. Palaeoecol.*, **260**, 77–91.

Ettensohn, F.R., Rast, N. & Brett, C.E. (2002) *Ancient Seismites. 359.* Geological Society of America, Boulder.

Fanetti, D., Anselmetti, F.S., Chapron, E., Sturm, M. & Vezzoli, L. (2008) Megaturbidite deposits in the Holocene basin fill of Lake Como (Southern Alps, Italy). *Palaeogeogr. Palaeoclimatol. Palaeoecol.*, **259**, 323–340. doi: 10.1016/j.palaeo.2007.10.014.

Farr, T.G., Rosen, P.A., Caro, E., Crippen, R., Duren, R. & Hensley, S. (2007) The Shuttle radar topography mission. *Rev. Geophys.*, **45**. RG2004, doi: 10.1029/2005rg000183.

© 2010 The Authors

Febrer, J.M., Plasencia, M.P. & Sabbione, N.C. (2000) Local and regional seismicity from Ushuaia broadband station observations (Tierra del Fuego). *Terra Antarct.*, **8**, 35–40.

Finckh, P., Kelts, K. & Lambert, A. (1984) Seismic stratigraphy and Bedrock forms in Perialpine Lakes. *Geol. Soc. Am. Bull.*, **95**, 1118–1128.

Garfunkel, Z. (1981) Internal structure of the dead Sea Leaky transform (Rift) in relation to plate kinematics. *Tectonophysics*, **80**, 81–108.

Girardclos, S., Fiore, J., Rachoud-Schneider, A.-M., Baster, I.R.A. & Wildi, W. (2005) Petit-Lac (Western Lake Geneva) environment and climate history from deglaciation to the present: a synthesis. *Boreas*, **34**, 417–433. doi: 10.1080/03009480500231385.

Goldfinger, C., Morey, A.E., Nelson, C.H., Gutiérrez-Pastor, J., Johnson, J.E., Karabanov, E., Chaytor, J. & Eriksson, A. (2007) Rupture lengths and temporal history of significant earthquakes on the offshore and north coast segments of the Northern San Andreas fault based on turbidite stratigraphy. *Earth Planet. Sci. Lett.*, **254**, 9–27.

Goldfinger, C., Nelson, C.H. & Johnson, J.E., Shipboard Sci Party. (2003) Holocene earthquake records from the Cascadia Subduction Zone and Northern San Andreas fault based on precise dating of offshore turbidites. *Annu. Rev. Earth Planet. Sci.*, **31**, 555–577. doi: 10.1146/annurev.earth.31.100901.141246.

Gordillo, S., Bujalesky, G.G., Pirazzoli, P.A., Rabassa, J.O. & Saliege, J.F. (1992) Holocene raised beaches along the Northern Coast of the Beagle Channel, Tierra-Del-Fuego, Argentina. *Palaeogeogr. Palaeoclimatol. Palaeoecol.*, **99**, 41–54.

Gordillo, S., Coronato, A.M.J. & Rabassa, J.O. (1993) Late quaternary evolution of a Subantarctic Paleofjord, Tierra Del Fuego. *Quat. Sci. Rev.*, **12**, 889–897.

Grant, L.B. & Sieh, K. (1994) Paleoseismic evidence of clustered earthquakes on the San Andreas fault in the Carrizo Plain, California. *J. Geophys. Res.*, **99**(B4), 6819–6841.

Guyard, A., St-Onge, G., Chapron, E., Anselmetti, F.S. & Francus, P. (2007) The AD 1881 earthquake-triggered slump and late holocene flood-induced Turbidites from Proglacial Lake Bramant, Western French Alps. In: *Submarine Mass Movements and their Consequences* (Ed. by V. Lykousis, D. Sakellariou & J. Locat), pp. 279–286. Springer, Berlin.

Hjelstuen, B.O., Haflidason, H., Sejrup, H.P. & Lysa, A. (2009) Sedimentary processes and depositional environments in Glaciated Fjord systems – evidence from Nordfjord, Norway. *Mar. Geol.*, **258**, 88–99. doi: 10.1016/j.margeo.2008.11.010.

Hogan, P. (2009) World Wind, Nasa Ames Research Center. Available at: http://www.worldwind.arc.nasa.gov. Retrieved January 12, 2009.

Jacoby, G.C., Sheppard, P.R. & Sieh, K.E. (1988) Irregular recurrence of large earthquakes along the San-Andreas fault – evidence from trees. *Science*, **241**, 196–199.

Jaschek, E., Sabbione, N. & Sierra, P. (1982) Reubicación De Sismos Localizados En Territorio Argentino (1920–1963). S. Geofisica, Observatorio Astronómico de la Universidad Nacional de La Plata. Tomo XI, No. 1.

Kastens, K.A. & Cita, M.B. (1981) Tsunami-induced sediment transport in the Abyssal Mediterranean-Sea. *Geol. Soc. Am. Bull.*, **92**, 845–857.

Kelts, K. & Hsu, K.J. (1980) Resedimented facies of 1875 Horgen Slumps in Lake Zurich and a process model of longitudinal transport of turbidity currents. *Eclo. Geol. Helv.*, **74**, 271–281.

Ken-Tor, R., Agnon, A., Enzel, Y., Stein, M., Marco, S. & Negendank, J.F.W. (2001) High-resolution geological record of historic earthquakes in the Dead Sea basin. *J. Geophys. Res.*, **106**(B2), 2221–2234.

Klepeis, K.A. (1994) The Magallanes and Deseado fault zones: major segments of the South American-Scotia transform plate boundary in Southernmost South America, Tierra Del Fuego. *J. Geophys. Res.*, **99**, 22001–22014.

Koinig, K.A., Shotyk, W., Lotter, A.F., Ohlendorf, C. & Sturm, M. (2003) 9000 years of geochemical evolution of lithogenic major and trace elements in the sediment of an Alpine Lake – the role of climate, vegetation, and land-use history. *J. Paleolimnol.*, **30**, 307–320.

Lodolo, E., Menichetti, M., Bartole, R., Ben-Avraham, Z., Tassone, A. & Lippai, H. (2003) Magallanes-Fagnano continental transform fault (Tierra Del Fuego, Southernmost South America). *Tectonics*, **22**, 1076–1102.

Lodolo, E., Menichetti, M., Tassone, A., Geletti, R., Sterzai, P., Lippai, H. & Hormaechea, J.L. (2002) Researchers target a continental transform fault in Tierra Del Fuego. *EOS Trans. AGU*, **83**(1), 1–6.

Lomnitz, C. (1970) Major earthquakes and Tsunamis in Chile during the period 1535–1955. *Int. J. Earth Sci.*, **59**, 938–960.

Marco, S. & Agnon, A. (1995) Prehistoric earthquake deformations near Masada, Dead-Sea Graben. *Geology*, **23**, 695–698.

Masson, D.G., Harbitz, C.B., Wynn, R.B., Pedersen, G. & Løvholt, F. (2007) Submarine landslides: processes, triggers and hazard prediction. *Philos. Trans. Roy. Soc. A: Math. Phys. Eng. Sci.*, **364**, 2009–2039. doi: 10.1098/rsta.2006.1810.

McCulloch, R.D., Bentley, M.J., Tipping, R.M. & Clapperton, C.M. (2005) Evidence for late-glacial ice dammed lakes in the Central strait of Magellan and Bahia Inutil, Southernmost South America. *Geogr. Ann., Ser. A: Phys. Geogr.*, **87**, 335–362. doi: 10.1111/j.0435-3676.2005.00262.x.

Menichetti, M., Lodolo, E., Tassone, A. & Geletti, R. (2001) *Neotectonics at the Magallanes-Fagnano Fault System (Tierra Del Fuego Island)*. Antarctic Neotectonics Workshop, Siena.

Migowski, C., Agnon, A., Bookman (Ken-Tor), R., Negendank, J.F.W. & Stein, M. (2004) Recurrence pattern of holocene Earthquakes along the Dead Sea transform revealed by varve-counting and radiocarbon dating of lacustrine sediments. *Earth Planet. Sci. Lett.*, **222**, 301–314.

Moernaut, J., De Batist, M., Charlet, F., Heirman, K., Chapron, E., Pino, M., Brummer, R. & Urrutia, R. (2007) Giant earthquakes in South-Central Chile revealed by Holocene mass-wasting events in Lake Puyehue. *Sediment. Geol.*, **195**, 239–256. doi: 10.1016/j.sedgeo.2006.08.005.

Monecke, K., Anselmetti, F.S., Becker, A., Schnellmann, M., Sturm, M. & Giardini, D. (2006) Earthquake-induced deformation structures in lake deposits: a late Pleistocene to Holocene Paleoseismic record for Central Switzerland. *Eclo. Geol. Helv.*, **99**, 343–362. doi: 10.1007/s00015-006-1193-x.

Monecke, K., Anselmetti, F.S., Becker, A., Sturm, M. & Giardini, D. (2004) The record of historic earthquakes in lake sediments of Central Switzerland. *Tectonophysics*, **394**, 21–40.

Moretti, M., Alfaro, P., Caselles, O. & Canas, J.A. (1999) Modelling seismites with a digital shaking table. *Tectonophysics*, **304**, 369–383.

Moy, C.M., Dunbar, R.B., Moreno, P.I., Francois, J.-P., Villa-Martínez, R., Mucciarone, D.M., Guilderson, T.P. & Garreaud, R.D. (2008) Isotopic evidence for hydrologic change related to the Westerlies in Sw Patagonia, Chile, during the last millennium. *Quat. Sci. Rev.*, **27**, 1335–1349.

© 2010 The Authors
Basin Research © 2010 Blackwell Publishing Ltd, European Association of Geoscientists & Engineers and International Association of Sedimentologists

Mulder, T. & Alexander, J. (2001) The physical character of subaqueous sedimentary density flows and their deposits. *Sedimentology*, **48**, 269–299.

Nakajima, T. & Kanai, Y. (2000) Sedimentary features of seismoturbidites triggered by the 1983 and older historical earthquakes in the Eastern Margin of the Japan Sea. *Sediment. Geol.*, **135**, 1–19.

Nesje, A. & Sejrup, H.P. (1988) Late Weichselian Devensian ice sheets in the North-Sea and adjacent land areas. *Boreas*, **17**, 371–384.

Oleskevich, D.A., Hyndman, R.D. & Wang, K. (1999) The updip and downdip limits to great subduction earthquakes: thermal and structural models of Cascadia, South Alaska, Sw Japan, and Chile. *J. Geophys. Res.*, **104**, 14965–14992.

Parsons, B., Wright, T., Rowe, P., Andrews, J., Jackson, J., Walker, R., Khatib, M., Talebian, M., Bergman, E. & Engdahl, E.R. (2006) The 1994 Sefidabeh (Eastern Iran) earthquakes revisited: new evidence from satellite Radar interferometry and carbonate dating about the growth of an active fold above a blind thrust fault. *Geophys. J. Int.*, **164**, 202–217. doi: 10.1111/j.1365-246X.2005.02655.X.

Piper, D.J.W., Cochonat, P. & Morrison, M.L. (1999) The sequence of events around the Epicentre of the 1929 Grand Banks earthquake: initiation of debris flows and turbidity current inferred from Sidescan Sonar. *Sedimentology*, **46**, 79–97.

Prentice, I.C., Guiot, J. & Harrison, S.P. (1992) Mediterranean vegetation, lake levels and Palaeoclimate at the last glacial maximum. *Nature*, **360**, 658–660.

Ricci Lucchi, F. (1995) Sedimentological indicators of paleoseismicity. In: *Perspectives in Paleoseismology*, **Vol. 6** (Ed. by L. Serva & D.B. Slemmons), pp. 7–17. Association of Engineering Geologists Special Publication, London.

Schnellmann, M., Anselmetti, F.S., Giardini, D. & McKenzie, J.A. (2005) Mass movement-induced fold-and-thrust belt structures in unconsolidated sediments in Lake Lucerne (Switzerland). *Sedimentology*, **52**, 271–289. doi:10.1111/j.1365-3091.2004.00694.x.

Schnellmann, M., Anselmetti, F.S., Giardini, D., McKenzie, J.A. & Ward, S.N. (2002) Prehistoric earthquake history revealed by Lacustrine slump deposits. *Geology*, **30**, 1131–1134.

Scholz, C.A. & Rosendahl, B.R. (1988) Low lake stands in Lakes Malawi and Tanganyika, East Africa, delineated with multifold seismic data. *Science*, **240**, 1645–1648. doi: 10.1126/science.240.4859.1645.

Shanmugam, G. (1997) The Bouma sequence and the Turbidite Mind Set. *Earth-Sci. Rev.*, **42**, 201–229.

Shiki, T., Cita, M.B. & Gorsline, D.S. (2000) Sedimentary features of seismites, seismo-turbidites and tsunamiites – an introduction. *Sediment. Geol.*, **135**, VII–IX.

Shteinman, B., Eckert, W., Kaganowsky, S. & Zohary, T. (1997) Seiche-induced resuspension in Lake Kinneret: a fluorescent tracer experiment. *Water Air Soil Pollut.*, **99**, 123–131.

Siegenthaler, C., Finger, W., Kelts, K. & Wang, S. (1987) Earthquake and seiche deposits in Lake Lucerne, Switzerland. *Eclo. Geol. Helv.*, **80**, 241–260.

Siegenthaler, C. & Sturm, M. (1991) Slump induced surges and sediment transport in Lake Uri, Switzerland. *Int. Assoc. Theor. Appl. Limnol. – Proc.*, **24**(2), 955–958.

Sims, J.D. (1975) Determining earthquake recurrence intervals from deformational structures in young lacustrine sediments. *Tectonophysics*, **29**, 141–152.

Stern, C.R. (2008) Holocene tephrochronology record of large explosive eruptions in the Southernmost Patagonian Andes. *Bull. Volcanol.*, **70**, 435–454.

St-Onge, G., Mulder, T., Piper, D.J.W., Hillaire-Marcel, C. & Stoner, J.S. (2004) Earthquake and flood-induced turbidites in the Saguenay Fjord (Quebec): a holocene paleoseismicity record. *Quat. Sci. Rev.*, **23**, 283–294. doi: 10.1016/j.quascirev.2003.03.001.

Strasser, M. & Anselmetti, F.S. (2008) Mass-movement event stratigraphy in Lake Zurich; a record of varying seismic and environmental impacts. *Beiträge zur Geol. Schw., Geotechn. Ser.*, **95**, 23–41.

Strasser, M., Anselmetti, F.S., Fah, D., Giardini, D. & Schnellmann, M. (2006) Magnitudes and source areas of large prehistoric Northern Alpine earthquakes revealed by slope failures in Lakes. *Geology*, **34**, 1005–1008.

Strasser, M., Stegmann, S., Bussmann, F., Anselmetti, F.S., Rick, B. & Kopf, A. (2007) Quantifying subaqueous slope stability during seismic shaking: Lake Lucerne as model for ocean margins. *Mar. Geol.*, **240**, 77–97.

Syvitski, J.P.M. & Schafer, C.T. (1996) Evidence for an earthquake-triggered basin collapse in Saguenay Fjord, Canada. *Sediment. Geol.*, **104**, 127–153.

Van Rensbergen, P., de Batist, M., Beck, C. & Chapron, E. (1999) High-resolution seismic stratigraphy of glacial to interglacial fill of a deep Glacigenic Lake: lake Le Bourget, Northwestern Alps, France. *Sediment. Geol.*, **128**, 99–129.

Vuan, A., Cazzaro, R., Costa, G., Russi, M. & Panza, G.F. (1999) S-wave velocity models in the Scotia Sea region, Antarctica, from nonlinear inversion of Rayleigh waves dispersion. *Pure Appl. Geophys.*, **154**, 121–139.

Waldmann, N., Ariztegui, D., Anselmetti, F.S., Austin, J.J.A., Dunbar, R., Moy, C.M. & Recasens, C. (2008) Seismic stratigraphy of Lago Fagnano sediments (Tierra Del Fuego, Argentina) – a potential archive of Paleoclimatic change and tectonic activity since the Late Glacial. *Geol. Acta*, **6**, 101–110.

Waldmann, N., Ariztegui, D., Anselmetti, F.S., Austin, J.J.A., Moy, C.M., Stern, C., Recasens, C. & Dunbar, R. (in press) Holocene climatic fluctuations and positioning of the Southern Hemisphere westerlies in Tierra Del Fuego (54°S), Patagonia. *J. Quat. Sci*. Doi: 10.1002/jqs.1263.

Waldmann, N., Ariztegui, D., Anselmetti, F.S., Coronato, A. & Austin, J.J.A. (2010) Geophysical evidence of multiple glacier advances in Lago Fagnano (54°S), Southernmost Patagonia. *Quat. Sci. Rev.*. doi: 10.1016/j.quascirev.2010.01.016.

Wallace, R.E. (1970) Earthquake recurrence intervals on San-Andreas fault. *Geol. Soc. Am. Bull.*, **81**, 2875–2889.

Weninger, B., Jöris, O. & Danzeglocke, U. (2009) Calpal, Cologne Radiocarbon Calibration & Palaeoclimate Research Package. Available at: http://www.calpal-online.de/. Retrieved January 12, 2009.

Winslow, M.A. (1982). The structural evolution of the Magallanes Basin and Neotectonics in the Southernmost Andes. Antarctic Geoscience. 3rd symposium on Antarctic geology and geophysics, Madison.

Manuscript received 3 September 2009; Manuscript accepted 6 April 2010.

© 2010 The Authors